Preprints (www.preprints.org) | NOT PEER-REVIEWED | Posted: 24 March 2022 doi:10.20944/preprints202202.0163.v2

Article

Estimating the Best Exponent of the Modified Universal Soil Loss Equation and Regionalizing the Modified Universal Soil Loss Equation Under Hydro-climatic Conditions of Ethiopia

Manaye Getu Tsige* [1], Andreas Malcherek [2] and Yilma Seleshi [3]

[1] Universität der Bundeswehr München; manaye.tsige@unibw.de
[2] Universität der Bundeswehr München; andreas.malcherek@unibw.de
[3] Addis Ababa University;yilmash@yahoo.com/yilma.seleshi@aau.edu.et
* Manaye Getu Tsige: getumanaye100@gmail.com/manaye.getu@astu.edu.et

Abstract: Soil erosion and sediment transport are quite complex processes as they depend on physical, biological, mechanical, and chemical processes within a particular catchment. Therefore, it is highly essential to better explain engaged physical processes and means of accounting for site-specific conditions, for soil loss and sediment yield estimation. This paper mainly focuses on physical explanations behind soil erosion and common soil erosion models like Universal or Revised Universal Soil Loss Equation(USLE/RUSLE) and Modified Universal Soil Loss Equation(MUSLE). Based on the physical explanations and overall limitations, the MUSLE is selected for the application of sediment yield estimation. The main objective of this paper is to estimate the best exponent of the MUSLE, and to estimate the best combination of the exponent and topographic factor of the MUSLE under hydro-climatic conditions of Ethiopia. For the sake of calibration procedure, the main parameters of the MUSLE which directly affect soil erosion process such as cover, conservation practice, soil erodibility, and topographic factors are estimated based on the past experiences from literature and comparative approaches, whereas the other parameters which do not directly affect the erosion process or which have no any physical meaning (i.e coefficient **a** and exponent **b**) are estimated through calibration. It is verified that the best exponent of the MUSLE is 1 irrespective of the topographic factor, which results in the maximum performance of the MUSLE (i.e approximately 100%). For the best combination of the exponent and topographic factor, the performance of the MUSLE is greater than or equal to 80% for all four watersheds under our consideration, we expect the same for other watersheds of Ethiopia.

Keywords: USLE; RUSLE, MUSLE; Ethiopia

1. Introduction

The fate of soil erosion and sediment transport can be seen in different ways. Sediment affects the water quantity and quality in rivers, lakes, and reservoirs [115]. This is because, quantity issues of sediment dynamics concern morphological aspects along with prevailing hydraulics to affect the aquatic habitats as well as the maintenance of flood control, navigable waterways and harbors as well as coastal protection [116]. In addition, quality issues relate to nutrients and hydrophobic pollutants associated with fine sediments to influence water quality, freshwater ecosystem services, human health, and management options such as dredging or dumping sediments [116]. Soil erosion and sediment transport can have a negative impact on poverty reduction and sustainable development. For example, it results in crop yield reduction in Sub-Saharan Africa [25]. If we particularly consider Ethiopia, soil erosion and sediment transport are some of the key problems for the sustainable development of the country. For example, it results in sedimentation of water supply, irrigation, and hydroelectric power reservoirs. Some of these sediment affected reservoirs are Koka hydroelectric Power reservoir [22],

© 2022 by the author(s). Distributed under a Creative Commons CC BY license.

Preprints (www.preprints.org) | NOT PEER-REVIEWED | Posted: 24 March 2022 doi:10.20944/preprints202202.0163.v2

Gilgel Gibe 1 hydroelectric Power Reservoir [24], Angereb water supply reservoir [23], Selamko and Shina irrigation reservoirs [28] and many more [30,31]. Furthermore, soil erosion leads to crop production reduction [26], lowers groundwater table [27], natural lake sedimentation [43,47,49] and economic loss [26,29] in Ethiopia.

Most of the tropical countries in the Eastern, Central and Southern Africa have no appropriate and accurate soil erosion models as was reviewed and pointed out by [120]. In Ethiopia, there is no commonly adopted soil erosion and sediment transport model; this may be because of limited hydrological and catchment data as it was reviewed and reported by [30,33,53]. However, soil erosion, sediment transport, deposition, consolidation and re-suspension are quite complex processes as they depend on physical, biological, mechanical and chemical processes within a particular catchment. Thus, the sedimentation processes are affected by weather and hydrological conditions, the temporal and spatial distribution of rainfall, rainfall intensity, hydraulics of flow, topography, density and pattern of land cover, impact of land use change [57], stream network, the types and extent of soil conservation and flood protection works, the temporal and spatial variation of soil physical properties, chemical properties and mineralogical constituents, biological properties and constituents, and soil mechanical properties. Some of these properties and constituents that affect soil erosion and sediment transport are soil texture [12,117], soil structure [12], particle density and volume fraction [64], pore size distribution [66], viscosity [67], bulk density [68], settling velocity [69], consistence [76], permeability [12], particle size distribution [64], soil moisture [60], gravel content [117], bed roughness [70], history of sediment bed formation and consolidation [71], cohesion [82], soil shear strength [83], compaction [65], gypsum content [54], calcium carbonate content [58], soil salinity [63], organic carbon content [55], soil hydrogen ion concentration (pH) [59], cation exchange capacity [73], soil base saturation [74], potassium, nitrogen and phosphorus fertilizers [75], organic matter content [56], Bioturbation [72], presence of micro-organisms like microphytobenthos [77], soil microbial biomass [80], macrofaunal species [81], biofilm formation [62], biochar [61], glomalin [78], antibiotics in the soil [79], Effect of Soil Management [125], etc.

Therefore, it is highly essential to better explain engaged physical processes and means of accounting for site-specific conditions, for soil loss and sediment yield estimation. Commonly used soil erosion models are Universal Soil Loss Equation (USLE) [12], Revised Universal Soil Loss Equation(RUSLE) [20] and Modified Universal Soil Loss Equation(MUSLE). In connection to these models, similar erosion models are RUSLE1, RUSLE2 [124] and the Chinese Soil Loss Equation (CSLE) [21]. The USLE is the foundation for others; it is used to estimate the annual soil loss from a field area, where the extent of erosion from sheet to rill erosion. However, it does not consider gully erosion, streambank erosion, streambed erosion, mudflow, massive land movement due to landslides or slumps. In fact, the USLE is an empirical soil loss model, is given by [12]:

$$A = RKLSCP$$

where, where A is soil loss in tons per acre per year, R is the rainfall erosivity factor in hundreds of foot-tons inches per acre per hour, K is the soil erodibility factor (in $0.01 * tons * acre * hour/acre * year * foot * tons * inch$), L is the slope length factor, S is the slope steepness factor or LS is the topographic factor, C is the cover factor, and P is the soil conservation practice factor.

Basically, the selection of soil erosion modelling techniques and approaches are based on data requirement and data availability (both quality and quantity of data), limitations of a model (basic assumptions and principles each model follows), and nature of the model (performance of the model at a specific condition). As part of the model selection criteria, we considered the physical explanation behind the above models, physical connection between factors, suitability of the models toward a specific location, and experiences of some other researchers about the important behavior of the models. Accordingly, the following limitations and advantages are drawn.

Preprints (www.preprints.org) | NOT PEER-REVIEWED | Posted: 24 March 2022 doi:10.20944/preprints202202.0163.v2

If we consider the physical explanation behind the models; the USLE/RUSLE depends on rainfall impact energy, and we expect soil detachment due to the rainfall impact. However, the rainfall impact or hammering also contributes to subsoil compaction, and it may reduce subsoil erosion. Yes, of course, we expect soil detachment due to the rainfall impact, however, we can not exactly tell in which direction a soil particle jumps or moves, where it reaches, or where measurement can be taken. Furthermore, the rainfall impact does not tell us how much energy is required to detach soil particles (soil strength or resistance against the rainfall impact energy). If the particle jumping due to the rainfall impact is not considered, it is the combined action of rainfall and runoff that causes soil erosion and sediment transport from a slope field, therefore, it is based on this principle that the amount of soil loss from the field can be measured at the bottom of the slope field. This is because, in the beginning of rain, more soil erosion due to the impact of rainfall and less sediment transport is expected. At the latter time, less soil erosion due to compaction but more sediment transport by runoff is expected. This can be a case particularly in the tropics where heavy rainfall compacts soil, infiltration decreases, runoff dominates quickly, and subsequently, more erosion in the beginning of rain is expected. As we said above the USLE/RUSLE/RUSLE2/CSLE considers the rainfall impact energy for soil detachment but it does not consider energy for sediment transport. The rainfall impact leads to sheet to rill erosion which mainly erodes topsoil. However, runoff concentration leads to gully formation (which erodes subsoil), riverbank erosion, and bedload transport.

If we consider the physical connection between factors, as far as we are talking about the rainfall impact energy for soil detachment; the physical connection between the rainfall erosivity, soil erodibility, topographic, cover, and conservation practice factors of the USLE/RUSLE is not convincing. One evidence for this is that, for instance, the soil cover factor reduces rainfall impact energy but the soil conservation practice factor does not reduce the impact energy of the rainfall.

If we consider the suitability of the models toward specific conditions or locations, in tropical Africa, the USLE and RUSLE are difficult to apply. This may be because unrealistic values were obtained for tropical soils from the equation's erodibility nomograph (Mulengera and Payton, 1999; Ndomba, 2007) as cited in [8]. It has also been observed that the table that was developed for estimating crop and soil management factors in the USA is inconsistent with farming practices in tropical Africa (Mulengera and Payton, 1999) as cited in [8].

If we consider data requirement and data availability, the USLE/RUSLE requires less than 30 minutes maximum rainfall intensity for its rainfall erosivity factor. We have daily rainfall data but we do not have 30 min rainfall data to test the USLE/RUSLE using its original data requirement; therefore, we can not minimize uncertainty. It is also required that the temporal and spatial distributions of rainfall should be captured at different points in a large watershed. This leads us to check whether the existing gauging stations are enough or not to capture the rainfall distributions of the watersheds under our consideration. In addition to several missing climatic data, the spatial distribution and density of the gauging stations are in question for the large watersheds of Ethiopia. Practically, it is not easy to test the USLE/RUSLE/ at the large watersheds in Ethiopia. However, the USLE/RUSLE was applied at different parts of Ethiopia following similar or different approaches to estimate any of its factors (e.g, [28,33–37,39–44,46,48]).

If we consider the experiences of some other researchers, the USLE/RUSLE is widely used with a combined sediment delivery ratio to calculate sediment yield at the outlet of a watershed. It has been observed that the delivery ratios to determine the sediment yield from the USLE can be predicted accurately but varies considerably [6]. The sediment delivery ratio varies with storms; the assumption of a constant sediment delivery ratio adds another source of error to the estimates as it was reviewed and reported by [5]. The reason for this may be due to the variation in rainfall distribution over time, from year to year [6]. The USLE is more accurate for soils with medium

Preprints (www.preprints.org) | NOT PEER-REVIEWED | Posted: 24 March 2022 doi:10.20944/preprints202202.0163.v2

texture and slopes of less than 400 ft in length with a gradient ranging between 3% and 18%, and it is managed with consistent cropping practices that are well represented in a plot scale erosion studies [12]. It is also warned that the farther these limits are exceeded, the greater will be the probability of significant extrapolation error [12]. For further reference, other problems connected to the USLE/RUSLE are discussed in [119].

Based on the above discussions, if we depend on runoff rather than rainfall, and if we take a measurement of runoff and sediment at one point (mainly at the outlet of a large watershed), then the modelling of sediment yield can be improved. This may be also because soil erosion depends on sediment being discharged with the flow; it varies with runoff and sediment concentration [119]. Furthermore, while considering runoff for the sediment yield modelling, we can take into account the effect of runoff shear stress for the sediment yield modelling [118]. Therefore, we proceed to consider the MUSLE which mainly depends on runoff energy for soil detachment and sediment transport. The runoff factor of the MUSLE represents the energy used in transporting as well as in detaching sediment, which acts as the best indicator for predicting sediment yield at individual storm events as it was reviewed and reported by (eg., [3,118]). Therefore, we expect soil detachment and sediment transport.

Williams (1975) developed the MUSLE using 778 storm-runoff events collected from 18 small watersheds [11,123], with areas varying from 15 to 1500ha, slopes from 0.9 to 5.9% and slope lengths of 78.64 to 173.74m (Hann et al.1994) as cited in [5]. The MUSLE is given by

$$y = a(Qq)^b KLSCP$$

where y is the sediment yield in metric tons, **a** is the coefficient and **b** is the exponent ($a = 11.8$ and $b = 0.56$ for USA, where the MUSLE was originally developed), Q is the runoff volume in m^3, q is the peak runoff rate in m^3/s, while the rest of its factors are similar to that of the USLE as we mentioned above. Basically, the MUSLE was developed for a small agricultural watershed, where the extent of erosion is from sheet to rill erosion, but gully erosion is still not considered. To apply the MUSLE for a large watershed (for our case, Hombole Watershed is 762,281ha, Mojo Watershed is 150,282ha, Gumera Watershed is 127,805ha and Gilgel Gibe 1 Watershed is 292,809ha), the approach that was proposed is using the MUSLE in Soil and Water Assessment Tool (SWAT) environment. This may be because sediment yield can be more accurately estimated if the large watershed is divided into subwatersheds (area < 2,590ha) to compensate for nonuniformly distributed sediment sources; the effect of watershed hydraulics and sediment particle size can be included by routing the sediment yield from subwatersheds to the large watershed [11].

If we consider the specific behavior of the MUSLE, it was analyzed that the greater appropriateness of field and direct measurements of runoff on a storm-event basis for better performance of the MUSLE output compared to use of indirect methods [5], and also the model provides appropriate estimates at a watershed rather than an experimental plot as it was reviewed and reported by [5]. In this connection if we consider SWAT, SWAT uses an indirect method (like Soil Conservation Service Curve Number) to generate runoff, then it uses the MUSLE to estimate soil loss from a hydrologic response unit (which is similar to a plot scale), then SWAT routes sediment output in channels to the outlet of a large watershed. But, this also leads to accumulative error at the end due to uncertainty in the definition of a channel, channel depth and width in the SWAT environment.

If we consider the experiences of some other researchers, the MUSLE is unsuitable for the prediction of sediment yield for small storms [118]. However, the slight variation in hydrological response of a watershed in terms of sediment yield might be changing in the antecedent hydrological conditions, the spatial and temporal distribution of rainfall, availability of eroded sediment throughout the watershed, which is not taken into account by the MUSLE as for many other lumped models [118].

Preprints (www.preprints.org) | NOT PEER-REVIEWED | Posted: 24 March 2022 doi:10.20944/preprints202202.0163.v2

If we consider the physical connection between factors of the MUSLE, as far as we are talking about runoff energy for soil detachment and sediment transport; the physical connection between the runoff, soil erodibility, topographic, cover, and soil conservation practice factors is convincing but further refining the physical connection between the factors may become necessary. For instance, the cover and soil conservation factors play a role to break runoff energy so as to protect soil loss due to runoff. As slope length becomes larger and larger, there is a possibility that erosion from the upper part of the slope gets deposited at the lower part of the slope (for instance, if we consider the last runoff from the slope field after the end of rainfall). This is because, depending on the magnitude of the runoff and its sediment transport capacity, the runoff takes up more soil particles and gets concentrated on its way to the bottom of the slope. In other words, the energy of the runoff decreases as resistance against flow increases along the length of the slope, and its shear force decreases.

If we consider the suitability of the model toward a specific location, the MUSLE has been observed to give good results in various applications in some parts of tropical Africa (Ndomba, 2007) as cited in [8], and it has been successfully demonstrated in sub-Saharan Africa [8]. As per the experimental plot result of sheet erosion at Enerta study site in Ethiopia, the MUSLE was better at estimating soil loss from a cultivated field than the USLE [121].

Therefore, based on the above limitations and advantages, the MUSLE should be tested at a watershed scale rather than a plot scale (which is similar to hru) under hydro-climatic conditions of Ethiopia, using directly measured flow data. In this regard, we have daily average flow records but we do not have daily peak flow records in our database. As we have discussed above the effect of the slope length factor on soil erosion and sediment transport should also be investigated. It follows that choosing and estimating the best parameters of the MUSLE, and regionalizing the MUSLE under hydro-climatic conditions of Ethiopia becomes important while considering the following cases.

If we consider the simulation time step, daily sediment yield may not reflect daily watershed information such as land cover, soil erodibility, and conservation activities. The reason for this can be soil erosion, sediment transport, deposition, consolidation ,and re-suspension are quite complex processes, which depend on physical, biological, mechanical, and chemical activities within a large heterogeneous watershed. Due to these complex processes, the soil that was eroded at an unknown last time can be transported, deposited, consolidated, re-suspended, and reached an outlet at a different time. Therefore, measured sediment at the outlet at the current time may not reflect the current information about the watershed; but may be unknown last time. This may be because sediment that was deposited along the length and the bottom of the slope by small runoff energy at a previous time, can be transported by high runoff energy at the current time. In the original development of the USLE, the annual soil erodibility factor was taken to compute the annual soil loss from the unit plot. Based on authors [12] formulation, we can conclude that the annual soil erodibility is the average of soil erodibility ranging from loose to compacted soil due to rainfall impact. As the soil erodibility factor of the USLE and MUSLE is the same, the annual time step is preferred over the daily time step (in the case of SWAT). Therefore, the annual simulation time step is selected to use the important features of the MUSLE; to take into account gully erosion (gully erosion is usually estimated on an annual basis [122]; it is important to note here is that gully erosion is a common problem in Ethiopia(eg.,[32,33,38,45,50])); to take into account overall gradual changing activities like cyclic behavior of agricultural activities, conservation practice, flood protection activities, plant growth and harvest with respect to rainfall pattern and extreme events in a one-year full cycle. And also to take into account quite complex processes of soil erosion, sediment transport, deposition, consolidation, and re-suspension at different seasonal variations of weather in a one-year full cycle. In connection to the simulation time step, if we see the experience of other researchers, for example, authors [10] estimated mean annual soil loss by regionalizing

Preprints (www.preprints.org) | NOT PEER-REVIEWED | Posted: 24 March 2022 doi:10.20944/preprints202202.0163.v2

the factors of the MUSLE for application to a data-scarce catchment in South Africa. The combination of MUSLE with other runoff models was tested on 26 watersheds in Texas with areas from 0.7 to 513km^2; these tests showed that the sediment-runoff model was feasible for predicting monthly and annual sediment yield [123].

If we consider the hydrologic response unit (hru) in the SWAT environment, as the number of hru becomes larger and larger, we better take into account spatial variability of land use, soil, and slope all over the watershed. To test the MUSLE at a watershed scale, sediment or flow routing in stream channels of SWAT is not considered (it is important to note here that there is uncertainty in the definition of a channel, channel width, and depth in the SWAT environment). Therefore, we only considered hrus to calculate the areal weighted average to capture the spatial variation of soil, cover, conservation practice and topography.

If we consider calibration parameters, all parameters ($a, b, Q, q, K, L, S, C, P$) of the MUSLE can potentially be used for calibration and validation [3]. In SWAT, **K** and **P** are calibration parameters. Authors [51] conducted global sensitivity analysis (Monte Carlo sampling) of the parameters of the MUSLE by using the extended Fourier amplitude sensitivity test (EFAST) method. Accordingly, the exponent b is the most sensitive parameter to predict the amount of soil loss, followed by **P**, **a**, **LS**, **C** and **q**, and **k's** influencing variables such as organic matter, soil structure class, and soil permeability class. In addition, authors [52] used Sobol's sensitivity analysis and found that the coefficient **a** and the exponent **b** are the most sensitive parameters of the MUSLE model contributing about 66% of the variability in the output sediment yield, at upper Malewa catchment in Kenya. On a storm event basis, authors [8] estimated the location parameters ($a = 12.4$ and $b = 0.51$) of the MUSLE for Ofuloko watershed in Nigeria. In some studies, only the exponent of the model was calibrated, which is logically more acceptable as it was reviewed and reported by [5]. The calibrated sediment does not reflect the actual soil erodibility and conservation practice factors on the ground unless otherwise they are measured. To accept our calibration, we should also check the calibrated value of the soil erodibility and conservation practice factors against the actual ones on the ground. This is because their product effect is reflected in the MUSLE rather than their individual effect during the calibration of sediment yield. Unless otherwise, we can not reach a certain conclusion that how these factors are really affecting the soil erosion process. For a given uniform watershed, the temporal variation of the soil erodibility, cover and conservation practice factors is expected. As the temporal variation of these factors is difficult to measure in a large watershed, we may estimate them through calibration. But, it is highly preferable if these factors are measured and studied at a temporal and spatial scale to understand their effect on soil erosion in a particular field. Any change in these factors affects the coefficient of the MUSLE, this is because only a product effect of the coefficient and these factors is reflected in the MUSLE rather than their individual effect during the calibration of sediment yield. As compared to the other parameters of the MUSLE, the individual effect of the exponent of the MUSLE is reflected during the calibration of sediment yield. Therefore, estimating the exponent of the MUSLE through calibration is more feasible than other parameters of the MUSLE. For a given uniform watershed, the topographic factor does not change with time (i.e it has a constant effect), the effect of the topographic factor can be seen when the MUSLE is applied at different watersheds. From this explanation, the independent effect of the exponent and topographic factor of the MUSLE can be seen by applying the model at different watersheds. Therefore, our main objective is to estimate the best exponent and topographic factor of the MUSLE by applying the model at different watersheds of Ethiopia. For the sake of calibration procedure, the main parameters of the MUSLE which directly affect soil erosion process such as cover, conservation practice, soil erodibility, and topographic factors are estimated based on the past experiences from literature and comparative approaches, whereas the other parameters which do

Preprints (www.preprints.org) | NOT PEER-REVIEWED | Posted: 24 March 2022 doi:10.20944/preprints202202.0163.v2

not directly affect the soil erosion process or which have no any physical meaning (i.e coefficient **a** and exponent **b**) are estimated through calibration.

It is verified that the best exponent of the MUSLE is 1 irrespective of the topographic factor, which results in the maximum performance of the MUSLE (i.e approximately 100%). For the best combination of the exponent and topographic factor, the MUSLE shows good performance (i.e greater than or equal to 80%) for all four watersheds under our consideration, we expect the same for other watersheds of Ethiopia.

2. Materials and Methods

2.1. Description of Study Areas

To begin our work, we considered four watersheds such as Gumera watershed in Abbay River Basin, Gilgel Gibe 1 watershed (at Assendabo) in Omo-Gibe River Basin, and Hombole and Mojo watersheds in Upper Awash River Basin, in Ethiopia. We describe the topography, hydro-climate, land use, and soil of the study areas based on the data which were prepared or obtained from different sources. Therefore, our description of the study area is based on the digital elevation models which were downloaded from the US Geological Survey; climatic data which were obtained from the National Meteorology Agency of Ethiopia; flow and sediment data which were obtained from the River Basin Authority of Ethiopia; soil and land use maps which were prepared from different sources by comparative and logical approaches. To identify the boundary of the river basin or watershed, streams are generated by delineating digital elevation model in SWATplus-QGIS plugin, and then the streams' shapefile is exported to the Google Earth Pro as Keyhole Markup Language to identify the outlet point of the watershed, and then the watershed is delineated by using its outlet point, and its shapefile is exported to the Google Earth Pro as Keyhole Markup Language to identify its geographic boundary(it is important to note that the delineated watershed should be surrounded by the streams that were generated at the previous step).

Preprints (www.preprints.org) | NOT PEER-REVIEWED | Posted: 24 March 2022 doi:10.20944/preprints202202.0163.v2

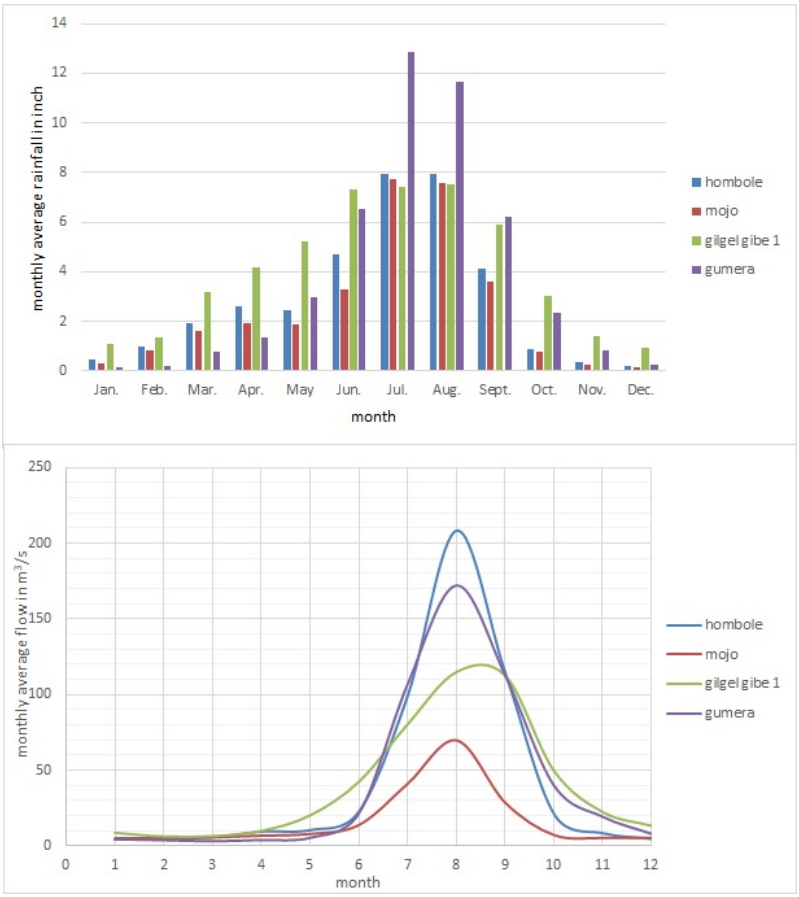

Figure 1. Monthly average rainfall, and monthly average outflow discharge at the main outlet point of each watershed under our consideration.

2.1.1. Upper Awash River Basin

Upper Awash River Basin drains into Koka hydroelectric power reservoir. Its geographic boundary lies between latitude 8.1036°N – 9.305°N and longitude 37.950°E – 39.295°E, and its main outlet point lies at latitude 8.468521°N and longitude 39.156143°E. The basin comprises two main gauged watersheds: Hombole and Mojo watersheds which cover 65.26% and 12.87% of the total area of the basin respectively, and the basin also includes an ungauged watershed which covers 21.87% of the total area of the basin. The total drainage area of the basin is estimated to be 11,680.25km^2.

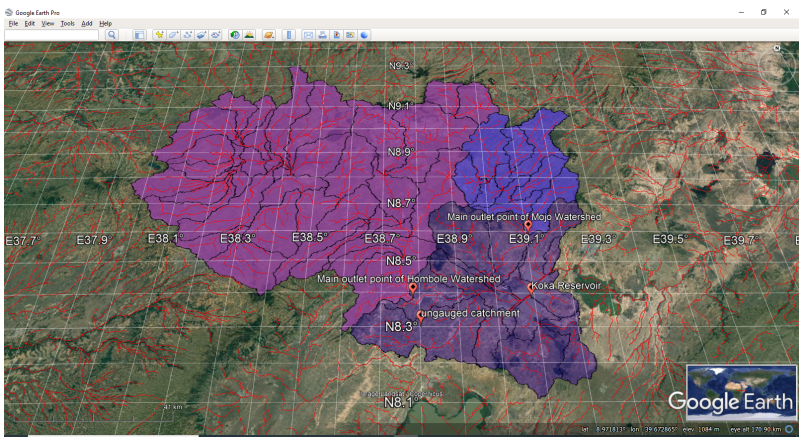

Figure 2. Hombole and Mojo watersheds in Upper Awash River Basin.

Preprints (www.preprints.org) | NOT PEER-REVIEWED | Posted: 24 March 2022 doi:10.20944/preprints202202.0163.v2

In the basin, there are active socio-economic activities like agricultural, industrial, and commercial activities. On the other angle, the basin experienced catastrophic flooding, and land degradation problems due to severe gully erosion. The gully erosion assessment in the basin was reported by [50]. Just to report average and extreme events in the basin based on the available records (it is important to note that missing records are not considered), the maximum daily rainfall was recorded over twenty-seven gauging stations within the record time period from 1986–2020 is 198.40 inches, and the average of the records is 2.82 inches. The list of these stations is given in the appendix A.1. The daily maximum and minimum temperatures were recorded over thirteen stations within the record time period from 1986–2020 are 43.40°C and -8.40°C, and the average of the maximum and minimum temperature records are 26.54°C and 10.90°C respectively. The list of these stations is given in the appendix A.1. The maximum and minimum relative humidity were recorded at either of the Addis Ababa (lat. 9.01891°N and log. 38.7475°E) or Debre Zeit stations (lat. 8.733333°N and log. 38.95°E) within the record time period from 1986–2012 are 100% and 1% respectively, and the average of the records is 58.23%. The maximum wind speed and the maximum sun hours duration were recorded at the Debre Zeit(AF) station within the record time period from 1994–2005 and 1994–2013 are 8.30m/s and 12.60hrs, and the average of the wind speed and sun hours duration records are 1.40m/s and 7.98hrs respectively.

For the Hombole watershed, the average, maximum and minimum elevations are 2,353.78m, 3,565m, and 1,698.94m above sea level respectively. The daily maximum and minimum outflow discharge were recorded at the main outlet of the watershed within the record time period from 1990–2016 are $803.10 m^3/s$ and $0.402 m^3/s$ respectively, and the average of the records is $43.20 m^3/s$ provided that the missing records are not considered. Monthly average rainfall, and monthly average outflow discharge at the main outlet point of the watershed are given in the figure 1 (it is to note that rainfall stations that lie inside and near the watershed, and those stations which have the record length from 15 to 35 years are considered to calculate a simple arithmetic average for the sake of comparison purpose). The maximum and minimum suspended sediment concentrations were recorded at the main outlet of the watershed within the record time period from 1989 to 2015 are $18.530 kg/m^3$ and $0.136 kg/m^3$ respectively, and the average of the records is $1.5 kg/m^3$ provided that only available records are considered. The dominant soil types are Eutric Vertisols and Haplic Nitisols which cover 57.30% and 17.77% of the total area of the watershed respectively. Land-use changes were observed in the watershed at four time periods, the dominant land use class is agricultural land; it covers 85.70% of the total watershed area in the time period from 1989 to 2000, 88.25% in the time period from 2001 to 2008, 86.52% in the time period from 2009 to 2012, and 86.26% in the time period from 2013 to 2015.

For the Mojo watershed, the average, maximum and minimum elevations are 2,140.4m, 2,932m, and 1,739.86m above sea level respectively. The daily maximum and minimum outflow discharge were recorded at the main outlet of the watershed within the record time period from 1990 – 2016 are $511.189 m^3/s$ and $0 m^3/s$ respectively, and the average of the records is $17.21 m^3/s$ provided that the missing records are not considered. Monthly average rainfall, and monthly average outflow discharge at the main point of the watershed are given in the figure 1 (it is to note that rainfall stations that lie inside the watershed, and those stations which have the record length from 15 to 35 years are considered to calculate the simple arithmetic average). The maximum and minimum suspended sediment concentrations were recorded at the main outlet point within the record time period from 1989 to 2015 are $37.66 kg/m^3$ and $0.16 kg/m^3$ respectively provided that only available records are considered. The dominant soil types are Vertic Cambisols and Eutric Vertisols which cover 46.80% and 45.06% of the total area of the watershed respectively. Land-use changes were observed in the watershed at four time periods; the dominant land use class is agricultural land; it covers 95.18% of the total watershed area in the time period from 1989 to 2000, 95.39% in the time period from 2001

Preprints (www.preprints.org) | NOT PEER-REVIEWED | Posted: 24 March 2022 doi:10.20944/preprints202202.0163.v2

to 2008, 93.85% in the time period from 2009 to 2012, and 93.82% in the time period from 2013 to 2015.

2.1.2. Gumera Watershed

Gumera watershed drains into Lake Tana. Its geographic boundary lies between latitude 11.574°N – 11.9052°N and longitude 37.6308°E – 38.1852°E , and its main outlet point lies at latitude 11.83°N and longitude 37.6299°E. The total drainage area of the watershed is estimated to be 1,278.05km^2. The average, maximum and minimum elevations are 2,260.45m, 3,654.33m, and 1,795.93m above sea level respectively.

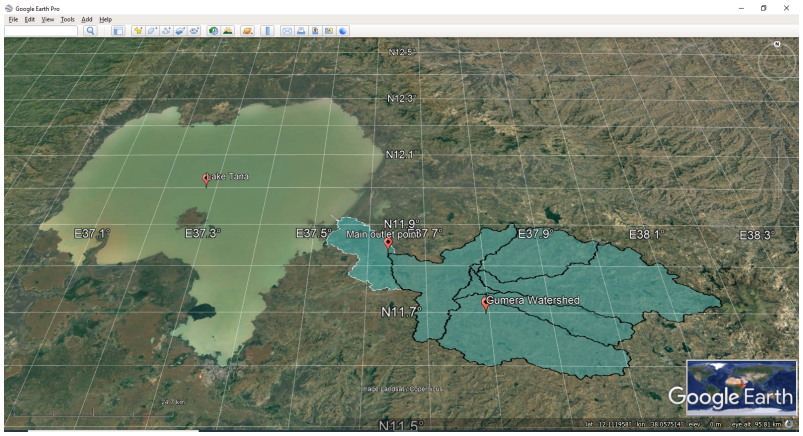

Figure 3. Gumera watershed in Abbay River Basin.

Just to report average and extreme events in the watershed based on available records (it is important to note that missing records are not considered), the maximum daily rainfall was recorded over seven gauging stations within the record time period from 1986 – 2020 is 147.1 inches, and the average of the records is 3.95 inches. These stations are listed in the appendix A.1. The daily maximum and minimum temperatures were recorded over five stations within the record time period from 1986 – 2019 are 39.7°C and -6.3°C , and the average of the maximum and minimum temperature records are 25.38°C and 10.02°C respectively. These stations are listed in the appendix A.1. The maximum and minimum relative humidity were recorded at Debre Tabor station (lat. 11.8666°N and log. 37.9954°E) within the record time period from 1988 to 2019 are 100% and 4% respectively, and the average of the records is 64.19%. The maximum wind speed and the maximum sun hours duration were recorded at the Debre Tabor station within the record time period from 1988 – 2018 and 1993 – 2019 are 18.3m/s and 11.7hrs, and the average of the wind speed and sun hours records are 1.1m/s and 7.01hrs respectively. The daily maximum and minimum outflow discharge were recorded at the main outlet of the watershed within the record time period from 2000 – 2017 are 307.937m^3/s and 0m^3/s respectively, and the average of the records is 44.97m^3/s. The maximum and minimum suspended sediment concentrations were recorded within the record time period from 1990 – 2017 are 10.07kg/m^3 and 0.17kg/m^3 respectively, and the average of the records is 3.43kg/m^3. Monthly average rainfall, and monthly average outflow discharge at the main outlet point of the watershed are given in the figure 1 (it is to note that rainfall stations that lie inside and near the watershed, and those stations which have the record length from 15 to 35 years are considered to calculate a simple arithmetic average). The dominant soil type is Haplic Luvisols which covers 69.50% of the total area of the watershed. Land-use changes were observed in the watershed at two time periods, the dominant land use class is agricultural land; it covers 84.33% of the total watershed area in the time period from 1989 to 2009, and 88.34% in the time period from 2010 to 2015.

Preprints (www.preprints.org) | NOT PEER-REVIEWED | Posted: 24 March 2022 doi:10.20944/preprints202202.0163.v2

2.1.3. Gilgel Gibe 1 Watershed

Gilgel Gibe 1 watershed drains into Gilgel Gibe 1 hydroelectric power reservoir. Its geographic boundary lies between latitude 7.3332°N – 7.995°N and longitude 36.515°E – 37.215°E, and its main outlet point lies at latitude 7.75°N and longitude 37.18299°E. The total drainage area of the watershed is estimated to be 2928.09km^2. The average, maximum and minimum elevations are 1,972.5m, 3,141.14m, and 80.4m above sea level respectively.

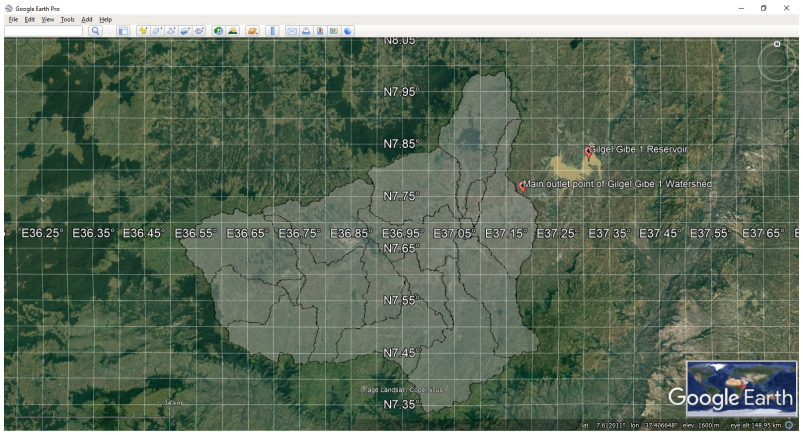

Figure 4. Gilgel Gibe 1 watershed in Omo-Gibe River Basin.

Just to report average and extreme records in the watershed based on available records (it is to note that missing records are not considered), the maximum daily rainfall was recorded over nine gauging stations within the record time period from 1986 – 2020 is 248.7 inches, and the average of the records is 4.37 inches. These nine gauging stations are listed in the appendix A.1. The daily minimum temperature was recorded over five stations within the record time period from 1986 – 2020 is 0°C, and the average of the maximum and minimum temperature records are 26.1°C and 12.47°C respectively. These five gauging stations are listed in the appendix A.1. The daily maximum and minimum outflow discharge were recorded at the main outlet of the watershed within the record time period from 2000 – 2015 are 269.54m^3/s and 1.67m^3/s respectively, and the average of the records is 40.97m^3/s. The maximum and minimum suspended sediment concentrations were recorded within the record time period from 1990 – 2017 are 0.90kg/m^3 and 0.12kg/m^3 respectively, and the average of the records is 0.43kg/m^3. Monthly average rainfall, and monthly average outflow discharge at the main outlet point of the watershed are given in the figure 1 (it is to note that rainfall stations that lie inside and near the watershed, and those stations which have the record length from 15 to 34 years are considered to calculate a simple arithmetic average). The dominant soil types are Humic Nitisols and Mollic Fluvisols which cover 52.86% and 25% of the total area of the watershed. Land-use changes were observed in the watershed at two time periods; the dominant land use class is agricultural land; it covers 90.23% and 91.953% of the total watershed area in the time period from 1989 – 2009 and 2010 – 2015 respectively.

2.2. Preparation of soil maps

Soil data is required to estimate the soil erodibility factor of the MUSLE. The necessities of preparing soil maps are to assign a specific type of soil from a general category of the soil, and to maintain the spatial variability of soil. For all our watersheds, national soil maps of Ethiopia which we obtained recently from the River Basin Authority of Ethiopia show us the general category of soil. To assign a specific type of soil, we locate the shapefile of each watershed on a harmonized world soil data map; we clip the harmonized world soil data map to the size of our watersheds in the QGIS environment. Then, we compare the national soil maps of Ethiopia, the harmonized world soil map, and the field observation report from the International Soil Reference and Information

Preprints (www.preprints.org) | NOT PEER-REVIEWED | Posted: 24 March 2022 doi:10.20944/preprints202202.0163.v2

Centre on QGIS. Particularly for the Upper Awash River Basin, we have two soil maps which were prepared at different times, from the River Basin Authority of Ethiopia. Based on these two soil maps, we maintain the spatial variability of soil just after the specific type of soil was assigned. We locate an areal coverage of the specific type of soil on the old map, that completely lies inside a large area of another specific type of soil on the current soil map. Then, we clip the specific type of soil on the current map to the size of the specific type of soil on the old map just to make a hole on the current soil map. Then, to obtain the final map, we add the specific type of soil on the old map to fill the hole of the current map. Therefore, soil maps of each watershed, which are finally prepared, are given in the figures 5, 6 and 7.

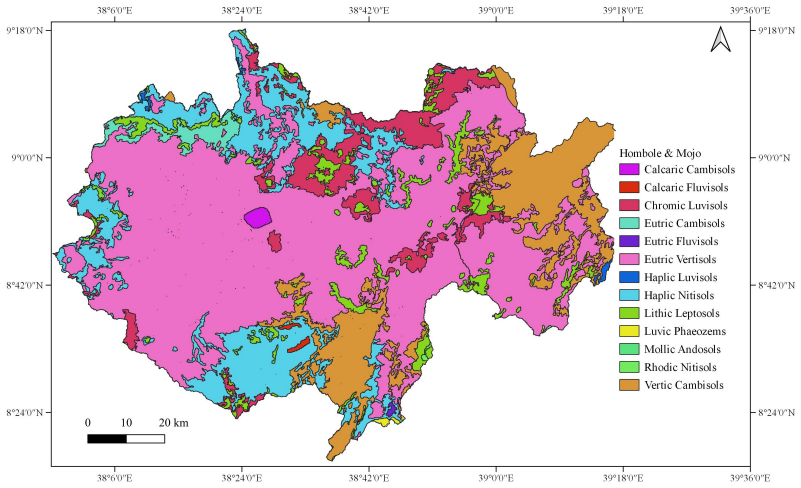

Figure 5. Soil maps of Hombole and Mojo Watersheds.

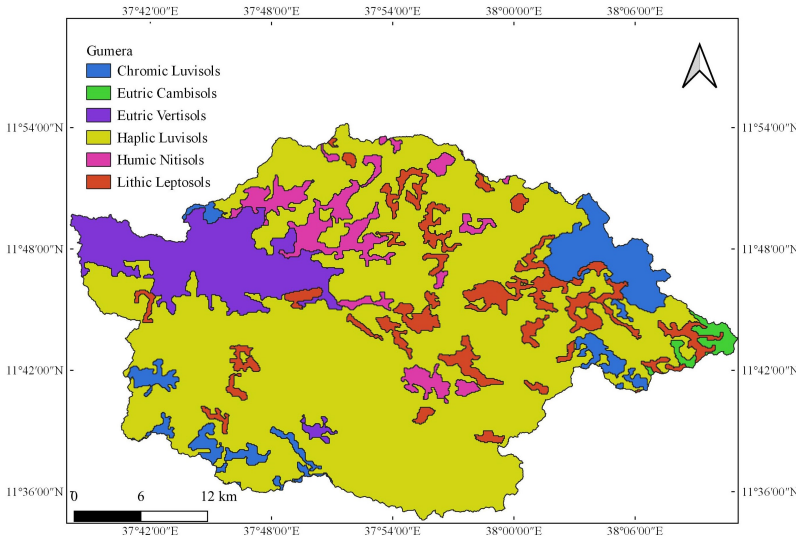

Figure 6. Soil map of Gumera Watershed .

Preprints (www.preprints.org) | NOT PEER-REVIEWED | Posted: 24 March 2022 doi:10.20944/preprints202202.0163.v2

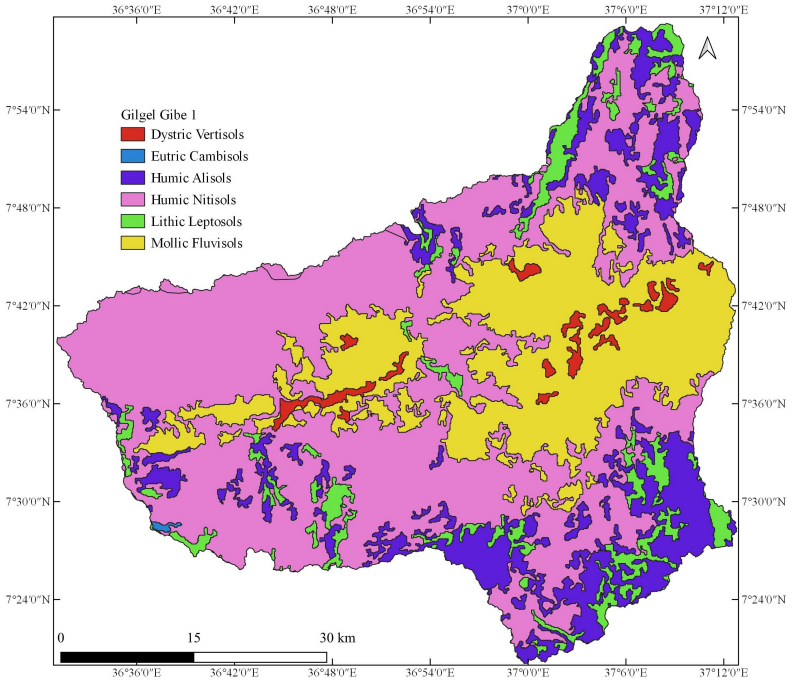

Figure 7. Soil map of Gilgel Gibe 1 watershed.

2.3. Preparation of land use maps

Preparation of land use data is necessary to estimate the cover and conservation practice factors of the MUSLE. Based on our assessment of land use and land cover by the support of Google Earth Pro, Planet Explorer, literature review (eg.,[84–87], and land use maps from the River Basin Authority of Ethiopia, land-use change has been observed in the study areas. As the basis of classification of land use maps, dominant land use classes are categorized at 30m spatial resolution. This is the acceptable level of spatial dimension to consider the spatial variability of land use at a tolerable level of accuracy. As a result, land use maps of each watershed are prepared based on a comparative approach and logical sequence. To prepare land use maps by the comparative approach, sample geographic coordinate points with its defined land use classes are collected from the Global land service map; the Normalized Difference Vegetation Index (NDVI) is prepared from the sample Landsat images to identify vegetation and bare land; easily observable urban, forest and agricultural land on historical imagery in the Google Earth Pro at different acquisition dates are digitized. A time demarcation of the land-use change classification depends on a number of available baseline land use maps per watershed; the time boundary of the Global land service maps, and acquisition dates of cloud-free sample Landsat satellite images and historical imagery in the Google Earth Pro. As a result, the time demarcation of land-use change for Hombole and Mojo watersheds are 1989 – 2000, 2001 – 2008, 2009 – 2012, 2013 – 2015, whereas for Gumera and Gilgel Gibe 1 watersheds are 1989 – 2009 and 2010 – 2015.

During the comparison of the above land use data files with the baseline national land use maps of Ethiopia on QGIS and Google Earth Pro; the vector data files are converted from the shapefile to the Keyhole Markup Language(KML) and vice versa. To prepare a land use map by the logical sequence, we check whether a change in land-use from one class to another is possible or not (for example, is the change from urban to agriculture possible?) as far as we are doing like comparison of different land use data files, which were prepared or acquired from different sources at the specified time demarcation. Particularly for the Upper Awash River Basin, land use classes which find on the previous baseline map but not on the latter map, are included on the latter map based on the logical sequence, and vice versa. And also missing land use classes like water bodies are added on either of the maps during the comparison of the maps with

Preprints (www.preprints.org) | NOT PEER-REVIEWED | Posted: 24 March 2022 doi:10.20944/preprints202202.0163.v2

other sources like historical imagery in the Google Earth Pro. While following these procedures, the land use maps which are finally prepared for each watershed are given in the figures 8, 9,10,11, 12,13, 14 and 15

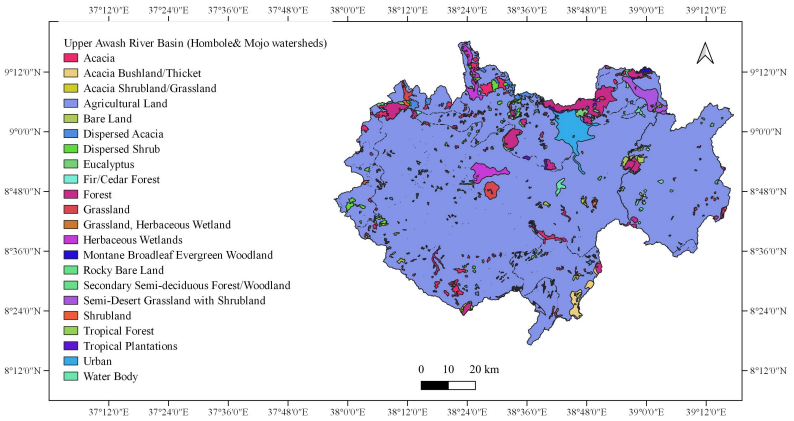

Figure 8. Land use map of Upper Awash River Basin (Hombole and Mojo Watersheds) from 1989 to 2000.

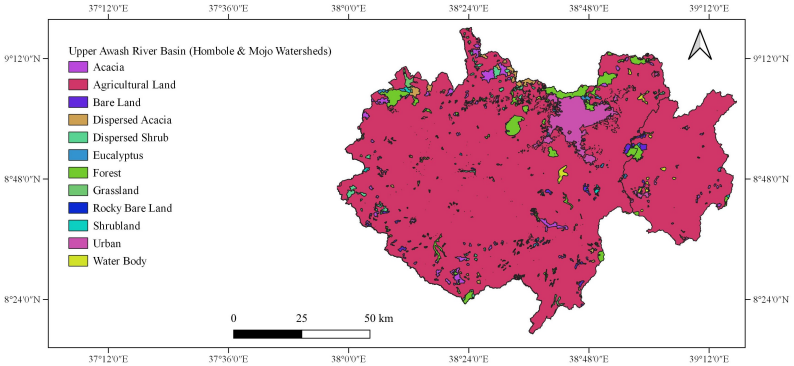

Figure 9. Land use map of Upper Awash River Basin (Hombole and Mojo Watersheds) from 2001 to 2008.

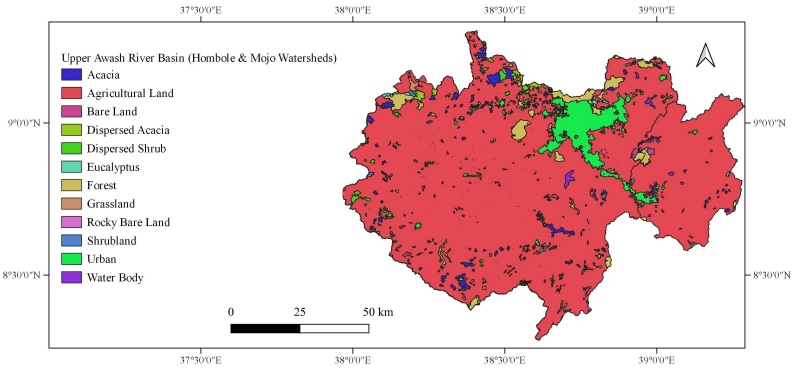

Figure 10. Land use map of Upper Awash River Basin (Hombole and Mojo Watersheds) from 2009 to 2012.

Preprints (www.preprints.org) | NOT PEER-REVIEWED | Posted: 24 March 2022 doi:10.20944/preprints202202.0163.v2

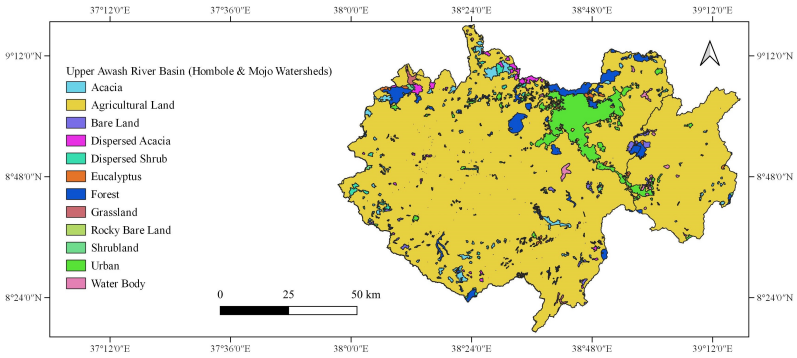

Figure 11. Land use map of Upper Awash River Basin (Hombole and Mojo Watersheds) from 2013 to 2015.

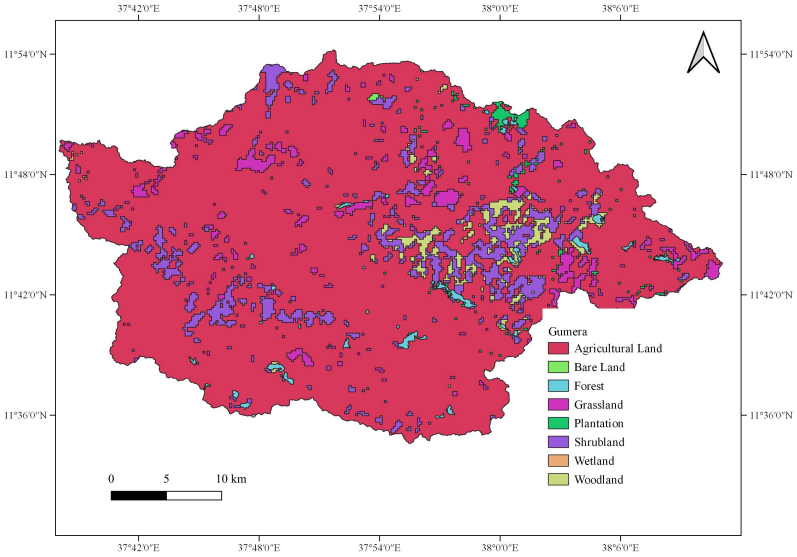

Figure 12. Land use map of Gumera Watershed from 1989 to 2009.

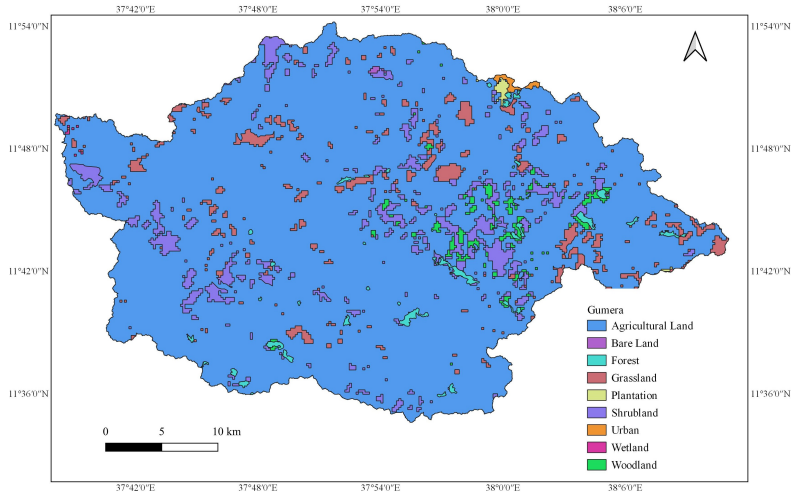

Figure 13. Land use map of Gumera Watershed from 2010 to 2015.

Preprints (www.preprints.org) | NOT PEER-REVIEWED | Posted: 24 March 2022 doi:10.20944/preprints202202.0163.v2

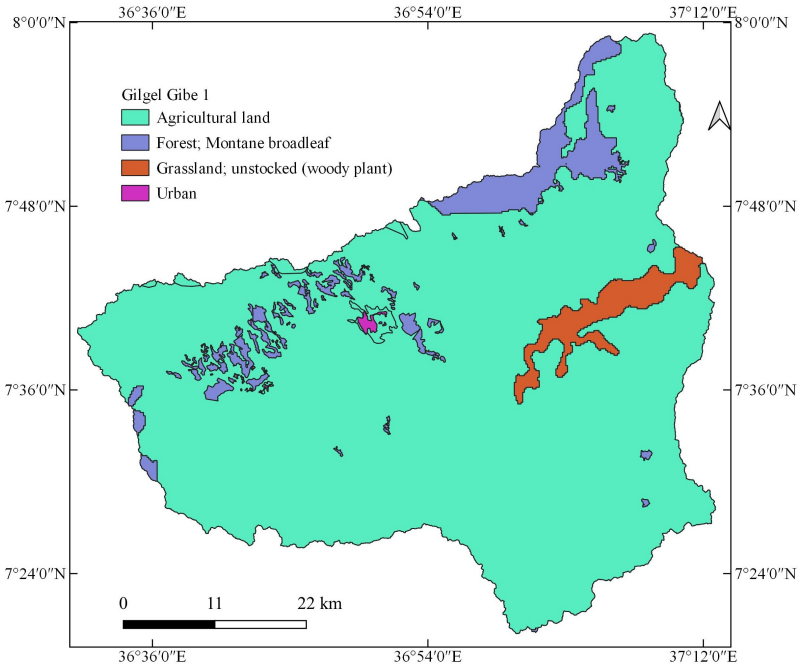

Figure 14. Land use map of Gilgel Gibe 1 Watershed from 1989 to 2009.

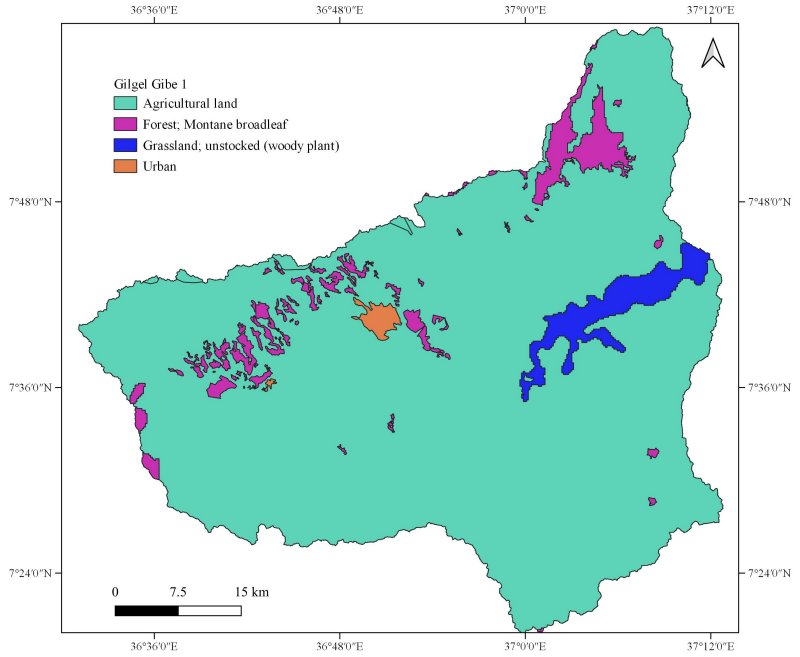

Figure 15. Land use map of Gilgel Gibe 1 Watershed from 2010 to 2015.

2.4. Sediment rating curves

A sediment rating curve is required to generate sediment data from corresponding flow data. The linear regression equation and nonlinear regression equations such as power function, the second and third-order polynomial function can be used to model the sediment rating curve(eg.,[96]). Different authors indicate that the power function is a commonly used nonlinear regression approach to model the sediment rating curve(eg.,[88,89,91]). The power function is given by:

$$C = aQ^b$$

where C is the suspended sediment load or concentration, Q is the discharge, a is the coefficient and b is the exponent. Different authors reviewed physical meanings

Preprints (www.preprints.org) | NOT PEER-REVIEWED | Posted: 24 March 2022 doi:10.20944/preprints202202.0163.v2

associated with the coefficient **a** and the exponent **b** (eg. [89,94,97]). Accordingly, the coefficient **a** represents an index of soil erodibility whereas the exponent **b** is considered as an index of erosivity and transport capacity of a river. Thus, the power function can be derived by interpreting or deducting the Modified Universal Soil Loss Equation (MUSLE), where its topographic, soil erodibility, cover and conservation practice factors describe a site-specific condition of a given watershed, and these factors affect the coefficient**a** of the power function at defined hydro-climatic conditions.

For the sake of simplicity of regression analysis, the nonlinear regression equation (in our case, the power function) can be transformed to the simple linear regression equation by log-transform of both sides of the nonlinear equation. Accordingly,
$logC = loga + blogQ$
If $y = logC$ and $x = blogQ$ then, $y = ax + b$
The Least Squares and Reduced Major Axis Line (R.M.A.L) regression methods can be applied to find the best-fit regression line on logarithms of suspended sediment load or concentration and discharge data, and back transform of the linear equation results in the power function. To find out the history and conceptual meaning related to the regression analysis and regression methods, readers are encouraged to refer [93,98]. Despite there are no generally accepted procedures to model the sediment rating curve, we proceed with the Least Squares regression method, which is based on the minimum sum of squared errors to estimate the coefficient **a** and the constant **b** of the best-fit linear regression equation on logarithms of suspended sediment concentration and discharge data.
$b = \frac{\sum_{i=1}^{n}(x_i-\bar{x})(y_i-\bar{y})}{\sum_{i=1}^{n}(x_i-\bar{x})^2}$
$a = \bar{y} - b\bar{x}$
Beside choosing sediment load-discharge [98], logged mean loads within discharge classes [97] or sediment concentration-discharge [96] approaches, correction factors($y = CF * aQ^b$) (eg.,[88,97]) and power function with some additive constant can be used ([88,95]) to improve the sediment rating curve. And also, to improve the sediment rating curve we may check data consistence or homogeneity test in order to find out data classes at specific hydro-climatic conditions.

While considering the above advantages and limitations to model the sediment rating curve, the relationship between discharge and suspended sediment concentration rate is checked against land-use change, seasonal weather variations or rainfall pattern, and period of land tillage. Accordingly, the sediment rating curve is drawn while considering rainfall and discharge relationship for Gilgel Gibe 1 watershed, shows some improvement provided that one extreme discharge $319.65 m^3/s$ on 8/23/2009 (no alike record in the daily average discharge from 1990–2015), which corresponds to the suspended sediment concentration $0.53 kg/m^3$, is removed from the records as part of the data quality check. And also, some data replication is possible to improve the sediment rating curve, due to the assumption that two measurements that are taken at very small time differences are almost the same as we only consider a pattern of record rather than a period of record, and also data record does not show watershed information. Accordingly, the sediment rating curve is drawn for the Gumera watershed, showing some improvement (the change in the coefficient of determination is from $R^2 = 0.324$ to $R^2 = 0.5091$) if it is a significant improvement. For the Hombole and Mojo watersheds, the sediment rating curves are drawn without any pre-conditions. This is because the above pre-conditions do not work for these two watersheds. For the Mojo watershed, two inconsistent records of the rainfall (extremely large and small), flow and sediment on Aug. 7, 1996 and Aug. 6, 2003, are removed from the records as part of the data quality check. Sediment rating curves of all watersheds are given in the figure 16.

Preprints (www.preprints.org) | NOT PEER-REVIEWED | Posted: 24 March 2022 doi:10.20944/preprints202202.0163.v2

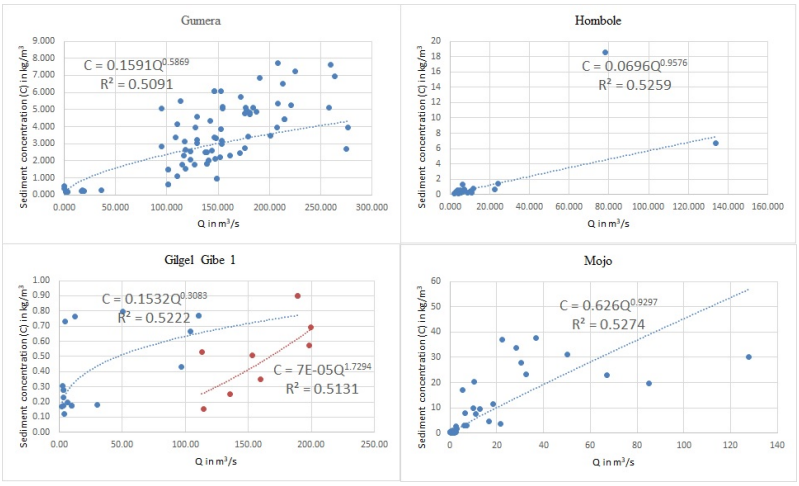

Figure 16. Sediment rating curve for each watershed under our consideration.

2.5. Estimating factors of the MUSLE

The original factors of the USLE represent the average value to estimate the annual sediment yield. The unit plot [12] represents the worst case for the maximum soil erosion at a given rainfall event. It is practically impossible to directly measure each field slope, slope length, the temporal variation of soil erodibility, instantaneous runoff, cover change and conservation practice for a large watershed. In the actual field, the field slope and length are not uniform, which means they are irregular. The topographic, and soil erodibility, cover and conservation practice factors depend on the spatial resolution of the digital elevation model (DEM), soil and land use maps respectively. Therefore, in the actual sediment modelling, average or weighted average of the field slope length [4] and slope steepness or simply topographic factor [3], average runoff, average soil erodibility factor [10], and average cover and conservation practice factors are taken.

Estimation of runoff factor

In the MUSLE, the runoff factor is the product of the total runoff volume and peak runoff rate. Authors [3] reviewed that the runoff factor represents the energy used in transporting as well as in detaching sediment, which acts as the best indicator for predicting sediment yield for the individual storm event. To estimate the runoff factor, the peak runoff rate and/or volume of runoff can be obtained by direct measurement of runoff on a storm-event basis, and also by using indirect methods such as Soil Conservation Service Curve Number (SCS CN) method, Rational method, flood routing, unit hydrograph, etc. For our case, we used the daily average discharge to estimate the annual total runoff volume and yearly peak runoff rate for the annual sediment yield estimation. The reasons for why we use directly measured flow data and why we estimate the annual sediment yield are addressed in the introduction section.

Estimation of soil erodibility factor (K-factor)

Authors [12] defined soil erodibility factor as the soil loss rate per erosion index unit for a specified soil as measured on a unit plot; the unit plot is defined as a 72.6-ft length of uniform 9-percent slope continuously in clean-tilled fallow; it is the continuous fallow tilled up and down the slope. The soil erodibility factor is given by[12]:

$$K = \frac{\sum_{n=1}^{N}(A)_n}{\sum_{n=1}^{N}(EI_{30})_n}$$

where A is the event soil loss from the unit plot in tons/acre/year, E is the storm kinetic energy in 100*foot-tons/acre, and I_{30} is the maximum 30 minutes intensity in inch/hour, K is the soil erodibility factor in $0.01 * tons * acre * hour/acre * year * foot * tons * inch$. It is important to note that the soil erodibility factor represents the worst or the maximum possible erosion from the unit plot with the specified field slope and length. At the same rainfall impact pressure, less soil erosion condition that is different from the worst condition takes into account the soil cover and conservation practice on the same field slope and length. On the unit plot or any unit plot for that matter, the temporal

Preprints (www.preprints.org) | NOT PEER-REVIEWED | Posted: 24 March 2022 doi:10.20944/preprints202202.0163.v2

and spatial variation of the soil erodibility depend on types of soil; the quite complex interaction of physical, biological, chemical, and mechanical processes. From the soil erodibility table or equations (see figure 17), we can reveal that the soil erodibility factor varies from 0–1, where 0 indicates the soil that is hard to erode, whereas 1 represents easily erodible soil by the same rainfall impact pressure under otherwise similar soil erosion conditions. From this range of the soil erodibility factor, we can conclude that soil erodibility refers to the degree of being easy to erode a given soil.

Soil erodibility factor (K-factor) can be estimated by direct field measurement, or by using different empirical equations or soil erodibility nomograph.

1. The K-factor that was originally developed at soil condition of USA [12]:
   $K = \frac{\{[2.1*M^{1.14}*(10^{-4})*(12-a)]+3.25*(b-2)+2.5*(c-3)\}}{100}$
   where K = soil erodibility in $0.01 * tons * acre * hour/acre * year * foot * tons * inch$; $M = (\%silt + \%veryfinesand) * (100 - \%clay)$; M =Particle-size parameter; silt (%) = percentage of silt; % very fine sand = percentage of very fine sand (0.1 to 0.05 mm); clay (%) = percentage of clay; a = percentage of organic matter; b = soil structure code used in soil classification, c = profile permeability class. For soils containing less than 70 percent silt and very fine sand, the nomograph [12] is used to solve the above equation.
   Some comments on this equation: we do not have a percentage of very fine sand in our database to test the equation. Our source of data is the harmonized world soil data which includes texture, reference soil depth, drainage class, available water capacity, sand, silt and clay fraction, bulk density, gravel content, organic carbon content, pH, cation exchange capacity, base saturation, total exchangeable bases, calcium carbonate content, gypsum content, sodicity, and salinity content. As land tillage and mechanical compaction (due to rainfall impact) change the structure of the soil; the structure of tilled, bare, or compacted soil varies at temporal and spatial scales. As soil permeability depends on soil texture and organic matter, their relationship should be explicitly shown. Unrealistic values were obtained for tropical soils from the equation's erodibility nomograph (Mulengera and Payton, 1999; Ndomba, 2007) as cited in [8].
2. The K-factor (Williams and Renard, 1983) as cited in[99] and similar equation in [104,105].
   $K = (0.2 + 0.3 * \exp(-0.0256 * S_a * (1 - \frac{s_i}{100}))) * (\frac{S_i}{c_L + s_i})^{0.3} * (1 - \frac{0.25c}{c + \exp(3.72 - 2.95c)}) * (1 - \frac{0.7S_N}{S_N + \exp(-5.51 + 22.9S_N)})$
   where S_a = sand (%); S_i = silt (%); C_L = clay (%); $S_N = 1 - (S_a/100)$; C = organic carbon
3. The K-factor that was tested at soil condition of the Philippine [100]:
   $K = \left[0.043 * pH + \frac{0.62}{OM} + 0.0082 * S - 0.0062 * C\right] * Si$
   where pH = pH of the soil; OM = organic matter (%); S = sand content (%); C = clay ratio =% clay / (% sand + % silt); Si = silt content = % silt /100
4. The K-factor that was originally developed at volcanic soil of Hawaii, USA (El-Swaify and Dangler, 1976) as cited in[20]:
   $K = -0.03970 + 0.00311 * x_1 + 0.00043x_2 + 0.00185x_3 + 0.00258x_4 - 0.00823x_5$
   where x_1: unstable aggregate size fraction (< 0.250mm)(%); x_2 = modified silt (0.002–0.1 mm) (%) * modified sand (0.1–2 mm) (%); x_3: % base saturation; x_4: silt fraction (0.002–0.050 mm) (%); x_5: modified sand fraction (0.1–2 mm) (%).
   comment: we do not have unstable aggregate size fraction or modified silt and sand data in our database to test the equation.

5. Williams (1995) proposed the following K-factor as cited in [106]:
   $K = f_{csand} * f_{cl-si} * f_{orgC} * f_{hisand}$
   $f_{csand} = 0.2 + 0.3\exp[-0.256m_s(1 - \frac{m_{silt}}{100})]$
   $f_{cl-si} = (\frac{m_{silt}}{m_c - m_{silt}})^{0.3}$

Preprints (www.preprints.org) | NOT PEER-REVIEWED | Posted: 24 March 2022 doi:10.20944/preprints202202.0163.v2

$$forgC = 1 - \frac{0.25 * orgC}{orgC + \exp[3.72 - 2.95 orgC]}$$

$$f_{hisand} = 1 - \frac{0.7(1 - \frac{m_s}{100})}{1 - \frac{m_s}{100} + \exp[-5.51 + 22.9(1 - \frac{m_s}{100})]}$$

6. other soil erodibility's equations are mentioned in [20,101,105–109,112].

To test the soil erodibility equations on the basis of the original definition of the soil erodibility by [12], the following conditions should be fulfilled. From the MUSLE,

$K = \frac{y}{a(Qq)^b * LSCP}$

where, K represents the worst condition for the maximum erosion case when the slope field length is 22.13m and the slope angle is 9%. In this case, no cover and conservation practices are employed in the field to give protection against soil erosion; the land is tilled up and down the slope, and therefore, the maximum erosion is expected. In the above equation, K represents the maximum erosion case when observed sediment yield (y) is due to soil erosion from a field with a specified slope length, slope angle, cover and conservation practice. If we take $C = P = 1$, K represents the maximum erosion from the field with the specified slope length and angle. However, our observed sediment yield does not represent the worst conditions for the maximum erosion case; we have some magnitude of cover and soil conservation practice to give protection against soil erosion, and land is not tilled up and down the slope. Therefore, in this case, K represents the minimum value as compared to the actual value that will be obtained from the soil erodibility equation for the worst conditions for the maximum soil erosion case (K_{eq}).

$K_{min} = \frac{y}{LSaQ^b} << k_{eq}$

For our watersheds, the minimum K value is calculated by replacing the annual sediment load, runoff volume, and topographic factor (the reasons for why we use the annual erodility factor are given in the introduction section). Based on the soil data we have, the actual soil erodibility factor is calculated by using the soil erodibility equations that were proposed by [106], [100],and Williams and Renard (1983) as cited in [99]. Accordingly, the graphs of the K-factor are shown in the figure 17.

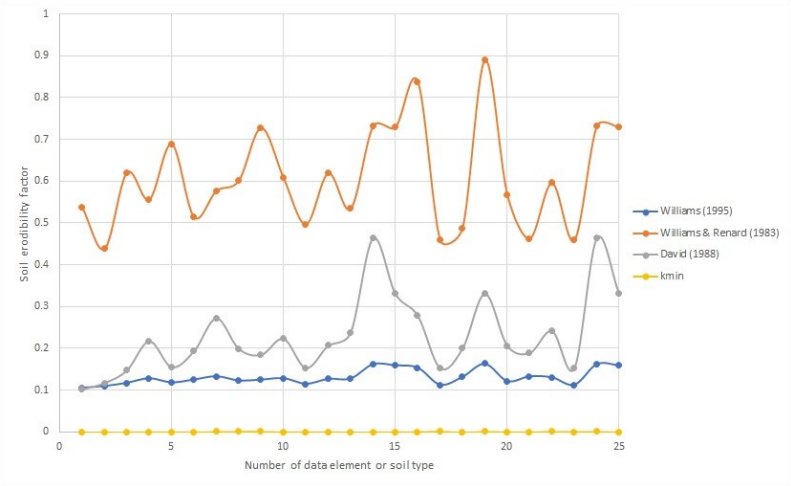

Figure 17. K-factor graphs of different soil types, which represent any of four watersheds under our consideration.

From the graph, a reasonable actual erodibility graph for our watersheds lies between the minimum K-factor graph and the calculated K-factor using Williams's (1995) equation as cited in [106]. To proceed with Williams's (1995) equation as cited in [106], Williams's sub-K-factors are calculated and compared based on silt and sand content, clay and silt continent, and organic carbon content of our soil data. In comparative speaking, soil erodibility increases if silt content increases, and sand and clay content decreases. This is because the interaction between soil particles ranges from the loose interaction for silt soil to the strong interaction for clay soil. Humus, manure, organic

Preprints (www.preprints.org) | NOT PEER-REVIEWED | Posted: 24 March 2022 doi:10.20944/preprints202202.0163.v2

matter, or organic carbon content decreases soil erodibility as it binds the soil particles together, or it provides protective cover for the soil particles.

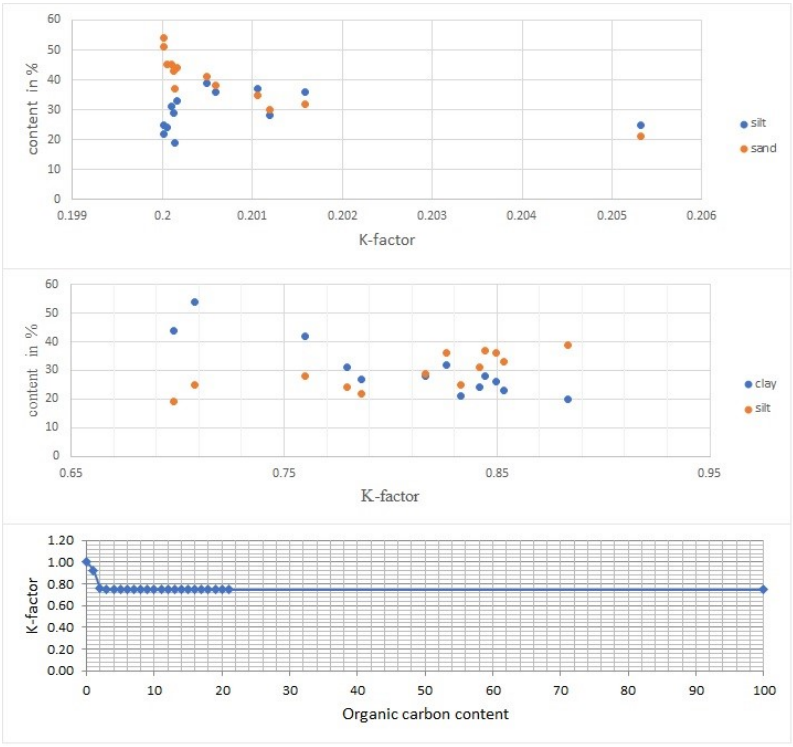

Figure 18. Comparison of sub-K-factors based on soil data, which represent any of four watersheds under our consideration.

From figure 18, the soil erodibility factors conform to the general comparisons stated above. Therefore, we use Williams's (1995) equation as cited in [106] to calculate the soil erodibility factor using soil data of the watersheds under our consideration, watersheds of Ethiopia in general.

Estimation of slope steepness and slope length factors

Slope steepness factor (S) is the ratio of soil loss from a field slope gradient to soil loss from the 9% slope under otherwise identical conditions [15]. A high rate of soil loss is associated with steep slopes [10,19], and soil loss prediction is more sensitive to the slope steepness than slope length [110].

Slope length is defined as the distance from the point of origin of overland flow to the point where either the slope gradient decreases enough that deposition begins, or the runoff water enters a well-defined channel that may be part of a drainage network or a constructed channel [12]. It is important to note that the definition of the slope length relies on the conditions at which the unit plot was constructed by [12]; the unit plot represents the worst condition for the maximum soil erosion case. Therefore, for the worst condition for the maximum erosion case, the slope length is the shortest distance from the origin of overland flow to the point where deposition takes place or enters stream channels. The slope lengths would rarely have a constant gradient along their entire length, and the slope irregularities would affect the amount of soil movement to the foot of the slope [12]. The slope length factor is given by [12]:

$$L = \left(\frac{\lambda}{\lambda_o}\right)^m$$

where λ is the slope length; λ_0 is the unit plot length = 72.6 ft = 22.13m. λ_0 is also defined as the horizontal projection of slope length (eg., [16–19]). In one term, slope steepness factor (S) and slope length factor (L) together is called topographic factor

Preprints (www.preprints.org) | NOT PEER-REVIEWED | Posted: 24 March 2022 doi:10.20944/preprints202202.0163.v2

(LS-factor). The topographic factor is the ratio of soil loss per unit area from a field slope length and gradient to that from the 22.1m length of uniform 9% slope under otherwise identical conditions [12]. Different equations have been suggested at different locations to estimate the topographic factor while taking into account site-specific conditions.

1. Topographic factor that was developed at the topographic condition of USA [12]:
   $LS = (\frac{\lambda}{72.6})^m(65.41sin^2\theta + 4.56sin\theta + 0.065)$
   where λ = slope length in feet; θ = angle of slope; m = dependent on the slope (0.5 if slope > 5%, 0.4 if slope is between 3.5% and 4.5% , 0.3 if slope is between 1% and 3%, 0.2 if slope is less than 1%).

2. McCool et al. (1987) improved the LS factor from classic USLE for use in terrain with steeper slopes as cited in[3], for use in RUSLE [19]:
   $L = \left(\frac{\lambda}{22.13}\right)^m$
   $m = \frac{\sin\theta}{\sin\theta + 0.269(\sin\theta)^{0.8} + 0.05}$
   $S = 3.0(\sin\theta)^{0.8} + 0.56\ for\ \lambda < 4m$
   $S = 10.8 * \sin\theta + 0.03 for \lambda > 4m and s < 9\%$
   $S = 16.8\sin\theta - 0.50\ for \lambda > 4m and s > 9\%$
   where λ is the slope length in meters, m is the dimensionless parameter, θ is the angle of field slope in degrees = tan-1 (s/100) and s is the field slope in percent.
3. Foster et al., (1977) and McCool et al., (1987, 1989) proposed the following equations for the calculation of the LS factors as cited in [20]
   $L = \left(\frac{\lambda}{72.6}\right)^m$
   $m = \frac{\beta}{1+\beta}$ (Foster et al.,1977) as cited in [20]
   $\beta = \frac{\frac{\sin\theta}{0.0896}}{3.0*(\sin\theta)^{0.8}+0.56}$ (McCool et al., 1989) as cited in[20]
   $S = 10.8 * \sin\theta + 0.03$ if slope (s) is less than 9% (McCool et al., 1987) as cited in[20]
   $s = 16.8sin\theta - 0.5$ if slope is greater than or equal to 9% (McCool et al, 1987) as cited in[20]
   $S = 3.0 * (\sin\theta)^{0.8} + 0.56$ if the slope length is shorter than 4.6m (McCool et al., 1987) as cited in [20], for the condition where water drains freely from slope end, and it is assumed that inter-rill erosion is insignificant on slopes shorter than 4.6m [19]. Where λ is the slope length (ft); θ is the angle of slope; m is the dependent on the slope (0.5 if slope > 5%, 0.4 if slope is between 3.5% and 4.5%, 0.3 if slope is between 1% and 3%, 0.2 if slope is less than 1%). As a remark, when conditions favour more inter-rill and less rill erosion, as in cases of consolidated soils like those found in no-till agriculture, m should be decreased by halving the β value, where a low rill to inter-rill erosion ratio is typical of conditions on rangelands [19]. With thawing, and cultivated soils dominated by surface flow, a constant value of 0.5 should be used (McCool et al., 1989, 1993) as cited in [19]. When freshly tilled soil is thawing, in a weakened state, and primarily subjected to surface flow, we use the following (McCool et al., 1993) as cited in [19].
   $S = 10.8\sin\theta + 0.03\ \ s < 9\%$
   $S = \left(\frac{\sin\theta}{0.0896}\right)^{0.6}\ \ s > 9\%$

4. The slope factor which is approximately equal to the LS factor at the topographic condition of the Philippines [100].
   $S = a + b * {S_L}^{4/3}$
   where S is the slope factor, a = 0.1; b = 0.21; SL is the slope in percent
5. The LS factor was developed at the topographic condition of Britain[102]:
   $LS = \left(\frac{\lambda}{22}\right)^{0.50} * \left(0.065 + 0.045s + 0.0065s^2\right)$
   where λ is the slope length (m); s is the slope steepness (%)

Preprints (www.preprints.org) | NOT PEER-REVIEWED | Posted: 24 March 2022 doi:10.20944/preprints202202.0163.v2

6. Apart from the LS factor of the USLE/RUSLE, the Chinese Soil Loss Equation [21] was developed while taking into consideration the Chinese soil environment and topographic conditions (including the modified equation that can calculate LS factor in >10° conditions) [13]. In the Chinese soil loss equation, the LS factor is calculated by [13].
$L = \left(\frac{\lambda}{22.1}\right)^{m}$
$m = 0.2 \ \ for\ \theta \leq 1.7\%$
$m = 0.3 \ \ for\ \ 1.7\% \ < \theta \leq 5.2\%$
$m = 0.4 \ \ for\ \ 5.2\% \ < \theta \leq 9\%$
$m = 0.5 \ \ for\ \theta > 9\%$
$S = 10.8 \sin\theta + 0.03 \ \ for\ \ \theta < 9\%$
$S = 16.8 \sin\theta - 0.05 \ \ for\ \ 9\% \leq \theta < 17.6\%$
$S = 21.9 \sin\theta - 0.96 \ \ for\ \theta \geq 17.6\%$
where λ is the slope length (m), m is the variable slope-length exponent, and θ is the slope angle (°).
7. other equations of the slope or slope length factor are mentioned in[3,7,13,21,103, 110,111].

To estimate the topographic factor (LS) for our watersheds, SWATplus is used to define as many hydrologic response units (hrus) as possible to consider an areal distribution of the slope steepness and slope length. In the TxtInOut folder of the SWATplus, area and topography information of each hru are stored in the hru and topography files respectively. These files are exported to an excel spreadsheet for analysis. The area, slope, and slope length of each hru are used to estimate the LS factor for each hru by using the above equations and the equations 1 and 2 stated below. The weighted average of the LS factors is taken to represent the watershed (it is important to note that the sediment or flow routing techniques in the SWATplus are not employed in this paper due to one or more reasons stated in the introduction section). The best-fit methods are chosen during the calibration of the annual sediment yield (see the calibration stage below).

Estimation of cover factor (C-factor)

It is the ratio of soil loss from a field with specified cropping to that from clean-tilled, continuous fallow under otherwise similar conditions. These similar conditions are; no soil conservation works (land is tilled up and down the slope), soil, slope steepness, slope length, and rainfall impact pressure is the same for both cropped field and fallow area. The C-factor is related to the land use and land cover, and it is the reduction factor to soil erosion vulnerability [14]. Therefore, the C-factor lies between 0 and 1, which describes the extent of vegetation cover to protect soil from erosion in a given catchment. Its value closer to 0 indicates dense vegetation cover, whereas its value closer to 1 indicates poor vegetation cover. Essentially, surface cover or canopy protects soil erosion by decreasing rainfall impact energy, but it may have less importance to protect sediment transport from a field. To some extent, we can say that surface cover affects soil erosion by reducing the transport capacity of the runoff water (Foster, 1982), and by causing deposition in ponded areas (Laflen, 1983) as cited in [20], and also by decreasing the surface area susceptible to raindrop impact [20]. In addition, plant root depth and distribution, and porosity increase the infiltration rate of rainfall water into the soil, and thus they play a role in reducing soil loss(Jeong et al. 2012) as cited in [113].

Although C-factor value can be taken from the literature or determined in situ, an extensive literature review compiling potential soil loss rates of different crop and forest covers compared to likely soil loss rates of bare soil can be used to determine likely C-factor values of a particular site [7]. The published guidelines [12,19], the revised C-factor (Cai et al., 2000) as cited in [114] and the Normalized Difference Vegetation Index [109,112] can be used to compute C-factor. For our case, the annual or average annual cover factor for each land use category is adopted based on the assessment of literature. Authors [7] reviewed C-factors for the general types of land use and land

Preprints (www.preprints.org) | NOT PEER-REVIEWED | Posted: 24 March 2022 doi:10.20944/preprints202202.0163.v2

cover. For our watersheds, the adopted cover factor for each land use is shown in the table 1. To estimate an areal weighted average of the cover factor for our watersheds, SWATplus is used to define as many hydrologic response units (hru) as possible to consider the areal distributions of land use and land cover. In the TxtInOut folder of the SWATplus, the area of each hru is stored in the hru file, and hru's land use data files are stored in the hru-data file. These files are exported to an excel spreadsheet for analysis and calculation of the areal weighted average. We can use the shapefile of each land use map (see figure 8, 9,10,11,12,13,14 and 15) to estimate the areal coverage of each land use classes in QGIS, and then the corresponding C and P-factors can be assigned.

Table 1. The assigned cover and conservation practice factors for each land use of the watersheds under our consideration

Land-use category	C-factor	P-factor
Acacia	0.01	1
Acacia Bushland/Thicket	0.01	1
Acacia Shrubland/Grassland	0.01	1
Agricultural land	0.525	0.52
Bare Land	1	1
Dispersed Acacia	0.01	1
Dispersed Shrub	0.01	1
Eucalyptus	0.001	1
Fir/Cedar Forest	0.001	1
Forest	0.001	1
Forest; Montane broadleaf	0.001	1
Grassland	0.01	1
Grassland, Herbaceous Wetland	0.01	1
Grassland; unstocked (woody plant)	0.01	1
Herbaceous Wetlands	0.01	1
Montane Broadleaf Evergreen Woodland	0.001	1
Rocky Bare Land	1	1
Secondary Semi-deciduous Forest/Woodland	0.001	1
Semi-Desert Grassland with Shrubland	0.01	1
Shrubland	0.01	1
Tropical Forest	0.001	1
Plantations	0.001	1
Tropical Plantations	0.001	1
Urban	0	1
Water Bodies	0	0
Wetland	0.01	1
Woodland	0.01	1

Estimation of soil conservation /erosion control practice factor (P-factor)

It is the ratio of soil loss associated with a specific support practice to the corresponding soil loss when cultivation is done up and down the slope [20] under otherwise similar conditions. The P-factor describes the effects of practices such as contouring, strip cropping, concave slopes, terraces, grass hedges, silt fences, straw bales, and subsurface drainage [14]. These conservation practices change the direction and speed of runoff [19]; it mainly reduces the transport of soil particles by blocking runoff and breaking its speed, but it does not reduce rainfall impact energy to reduce soil erosion. Therefore, the P-factor ranges from 0 to 1, where 0 represents the strong conservation practice (no soil loss from a field is expected), whereas 1 represents the worst condition for the maximum erosion due to lack of conservation practice and when land is tilled up and down the slope, and runoff takes the shortest well-defined channel or route in the field.

The difficulty of accurately mapping support practice factors or not observing support practices leads to many studies ignoring it by giving their P-factor a value of 1.0 [7]. Some P-factors can be ignored if some C- factors already account for the presence of a support factor such as intercropping or contouring [7]. All non-agricultural lands were

Preprints (www.preprints.org) | NOT PEER-REVIEWED | Posted: 24 March 2022 doi:10.20944/preprints202202.0163.v2

also assigned a value of 1 if no feasible conservation measures were applied [10,113,114]. At suitably detailed scales and with enough knowledge of farming practices, using the P-factor may lead to a more accurate estimation of soil loss [7]. Authors[5] reviewed that considering the temporal variation of the P-factor could significantly improve the performance of the MUSLE, although it has been rarely taken into account. The soil conservation or erosion control practice factors can be estimated with the help of available tables [12], using land use and land cover maps [10,113,114] and through field measurement (see literature review report in [5]. For our case, the annual soil conservation practice factor for each land use category is adopted based on the assessment of literature. Authors [7] reviewed P-factors for general types of land use and land cover. The adopted P-factor for land use and land cover category of each watershed is shown in the table 1. The areal weighted average of the P-factor is done in the same way as the cover factor.

Estimation of coefficient a and exponent b through calibration

For a chosen value of the exponent **b**, the best-fit corresponding value of the coefficient **a** is estimated through calibration. The selection of the best exponent and the best equation among listed above and below (see equations 1 and 2) for the topographic factor is done after calibration of observed and simulated sediment (i.e the MUSLE is used to estimate sediment load). The figure 19 shows sample graphs of the sediment calibration when the topographic factor is calculated using the equation that was proposed by [12].

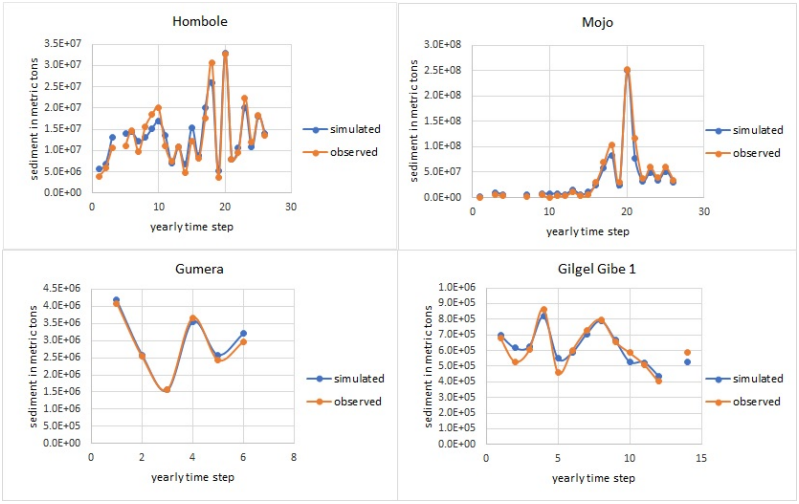

Figure 19. Observed and simulated sediment.

During calibration, Nash-Sutcliffe efficiency corresponds to each LS factor, the exponent **b** and the coefficient **a** is evaluated, and graphs of the exponent **b** versus Nash-Sutcliffe efficiency, and graphs of the coefficient **a** versus exponent **b** are drawn for each watershed, as shown in the figures 20,21,22,23,24,25 and 26. For a chosen value of **b**, we test seven different equations of the topographic factor for each watershed. Therefore, we can have as many graphs as possible.

Preprints (www.preprints.org) | NOT PEER-REVIEWED | Posted: 24 March 2022 doi:10.20944/preprints202202.0163.v2

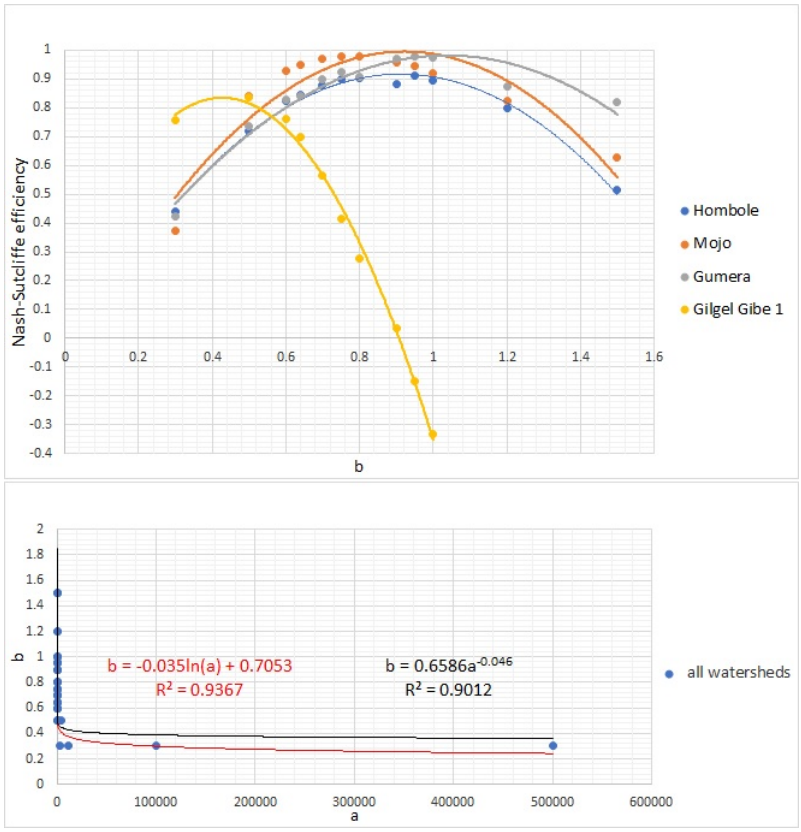

Figure 20. The relationship between exponent **b** versus Nash-Sutcliffe efficiency, and the coefficient **a** versus the exponent *b* when the topographic factor is calculated by using the equation that was proposed by [12].

Preprints (www.preprints.org) | NOT PEER-REVIEWED | Posted: 24 March 2022 doi:10.20944/preprints202202.0163.v2

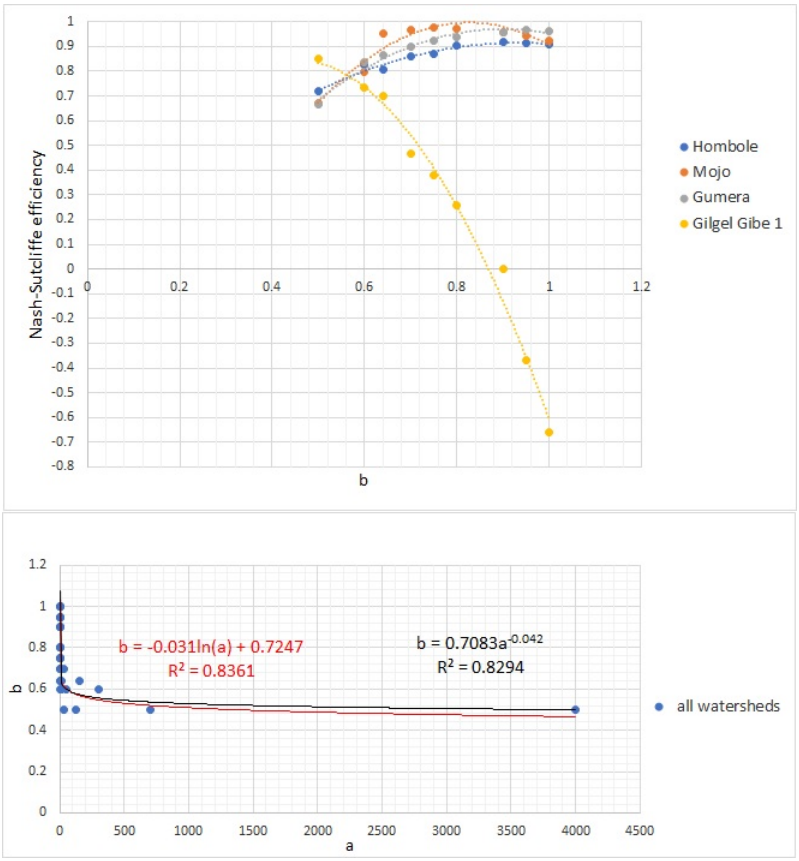

Figure 21. The relationship between exponent **b** versus Nash-Sutcliffe efficiency, and the coefficient **a** versus the exponent **b** when the topographic factor is calculated by using the equation that was proposed by [20].

Preprints (www.preprints.org) | NOT PEER-REVIEWED | Posted: 24 March 2022 doi:10.20944/preprints202202.0163.v2

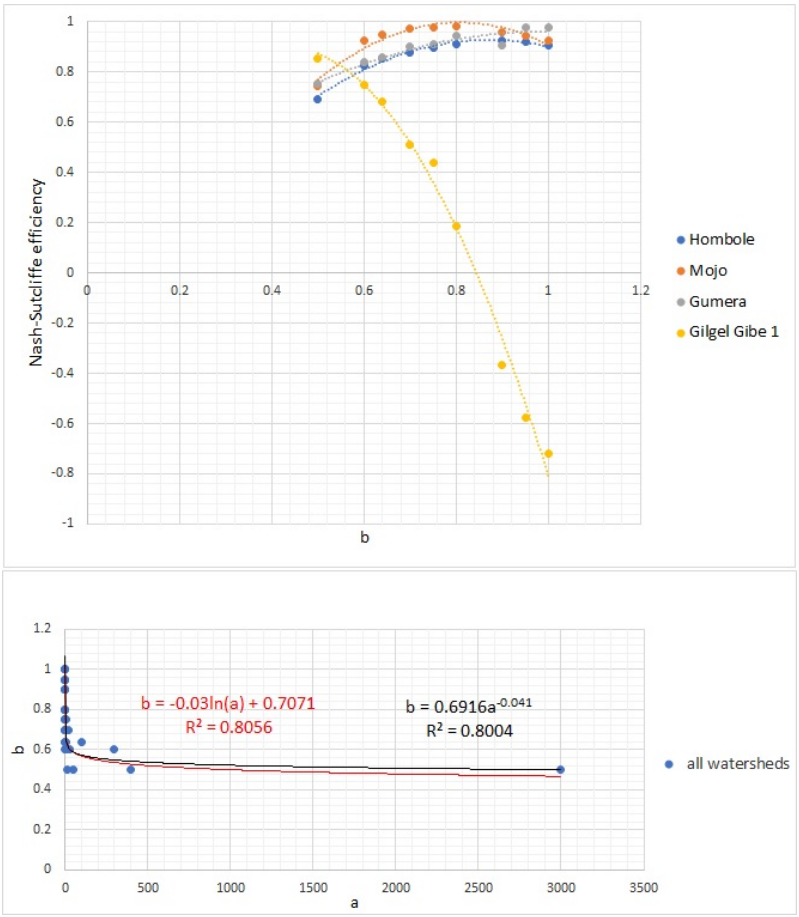

Figure 22. The relationship between exponent **b** versus Nash-Sutcliffe efficiency, and the coefficient **a** versus the exponent **b** when the topographic factor is calculated by using the equation that was proposed by [102].

Preprints (www.preprints.org) | NOT PEER-REVIEWED | Posted: 24 March 2022 doi:10.20944/preprints202202.0163.v2

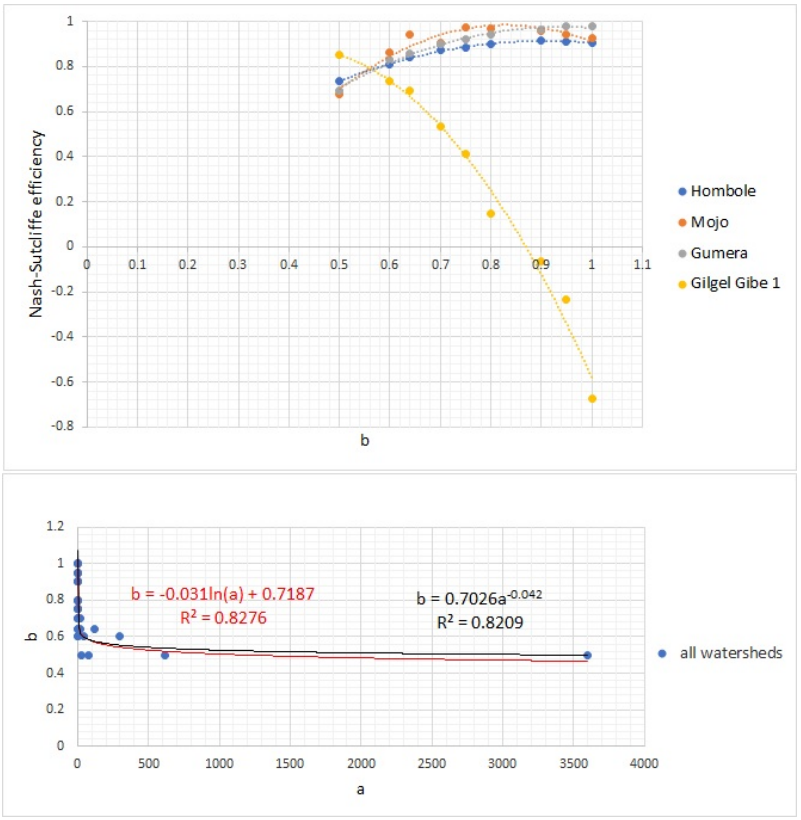

Figure 23. The relationship between exponent **b** versus Nash-Sutcliffe efficiency, and the coefficient **a** versus the exponent **b** when the topographic factor is calculated by using the equation that was proposed by McCool et al., (1987) as cited in [3].

Preprints (www.preprints.org) | NOT PEER-REVIEWED | Posted: 24 March 2022 doi:10.20944/preprints202202.0163.v2

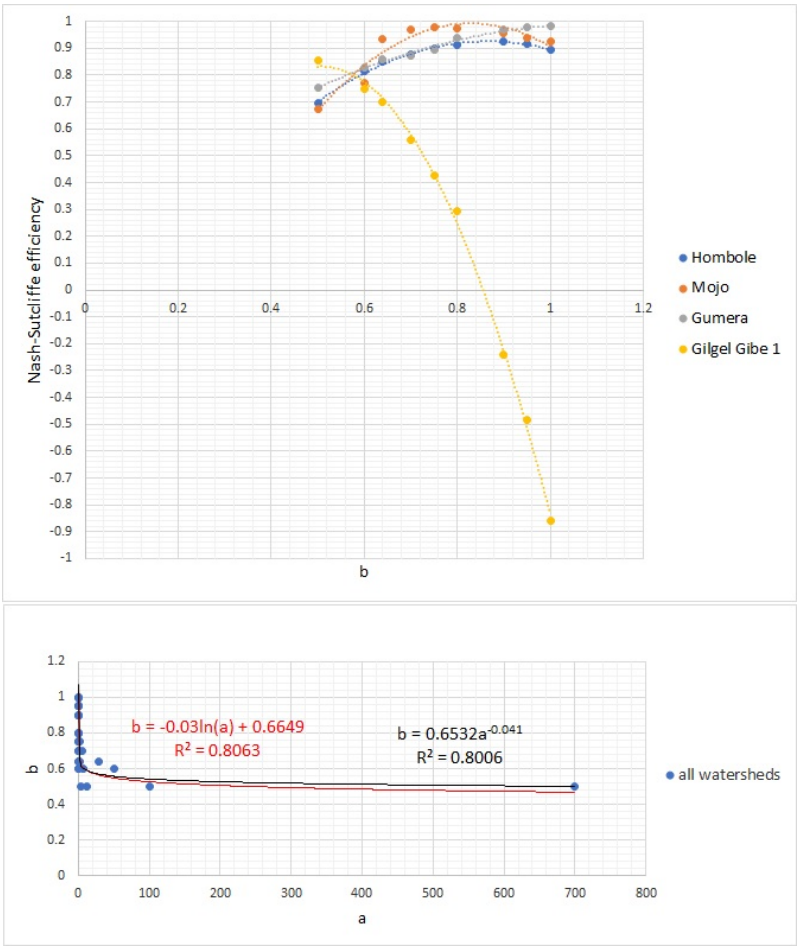

Figure 24. The relationship between exponent **b** versus Nash-Sutcliffe efficiency, and the coefficient **a** versus the exponent *b* when the topographic factor is calculated by using the equation that was proposed by[100].

Preprints (www.preprints.org) | NOT PEER-REVIEWED | Posted: 24 March 2022 doi:10.20944/preprints202202.0163.v2

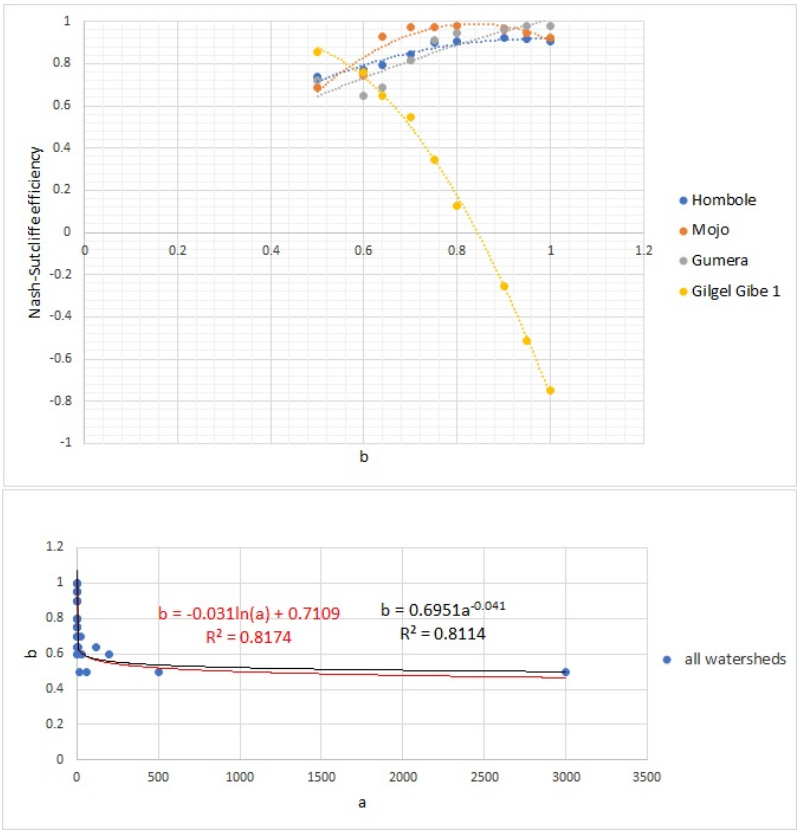

Figure 25. The relationship between exponent **b** versus Nash-Sutcliffe efficiency, and the coefficient **a** versus the exponent **b** when the topographic factor is calculated by using the Chines equation.

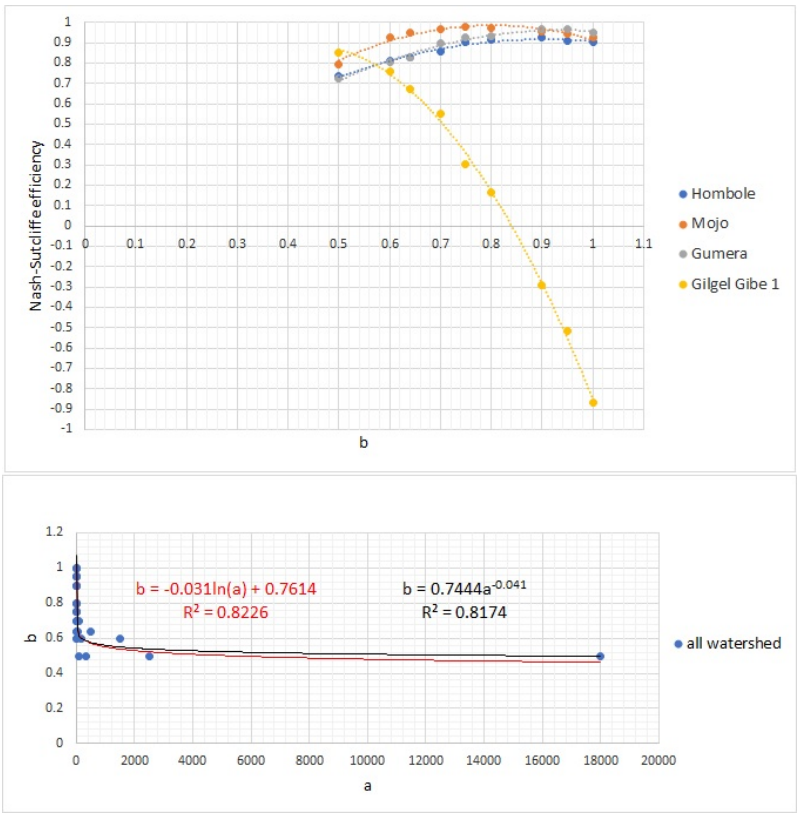

Figure 26. The relationship between exponent **b** versus Nash-Sutcliffe efficiency, and the coefficient **a** versus the exponent **b** when the topographic factor is calculated by using the equations 1 and 2

Preprints (www.preprints.org) | NOT PEER-REVIEWED | Posted: 24 March 2022 doi:10.20944/preprints202202.0163.v2

$$LS = (0.02222J^{1.5} + 0.03231J + 0.1004) * 0.2901 \triangle y^{0.4002} \; for \; J < 5\% \quad (1)$$

$$LS = (0.02222J^{1.5} + 0.03231J + 0.1004) * 0.2105 \triangle y^{0.5004} \; for \; J > 5\% \quad (2)$$

where J is the slope in %, $\triangle y$ is the slope length. For description, readers are encouraged to watch it at https://www.youtube.com/watch?v=w6w8jxbTJfo. For the case of the watersheds under our consideration, we take $\triangle$y/22.1 as the field slope length.

2.6. *Verifying the best exponent of the Modified Universal Soil Loss Equation*

As we have discussed in the introduction section, the yearly simulation time step is preferred to address the gradual processes of soil erosion and sediment transport. It is important to prove whether a change in the simulation time step changes the coefficient and the exponent of the MUSLE or not. This approach leads us to find the best exponent of the MUSLE.

Proof. If we consider the small simulation time step and the small simulation period, we can maintain the temporal variation of the factors which directly affect soil erosion process. For a given field, no change in the cover, conservation practice, and soil erodibility factors of the MUSLE will be expected at the small simulation period. At the end of the simulation period, only in variation of the coefficient and the exponent of the MUSLE with the simulation time step affect sediment yield output (look proof steps below, for a change in runoff and the peak runoff rate). If the variations of the coefficient and the exponent of the MUSLE with a small change in the simulation time step are detected, then the variations of the coefficient and the exponent with any other simulation time step are confirmed. For the sake of start, let us consider 1 and 2 unit simulation time steps and 2 unit simulation period; no change in the factors of the MUSLE will be expected for about 2 unit simulation period. Therefore, soil loss from a field at the 1 unit simulation time step for about 2 unit simulation period, is equal to the sum of soil loss at the end of the first and next 1 unit time;
$a_1(Q_1q_1)^{b_1}KLSCP + a_1(Q_2q_2)^{b_1}KLSCP$
where suffixes 1 and 2 indicate the first and second simulation at the 1 unit simulation time step or interval. It is to note that K, L, S, C, and P are the same for the 2 unit simulation period; the coefficient and the exponent are the same at the 1 unit simulation time step.
Soil loss from the field at the 2 unit simulation time step for about 2 unit simulation period;
$a_2((Q_1 + Q_2)q_1)^{b_2}KLSCP$ if the peak runoff rate is q_1
$a_2((Q_1 + Q_2)q_2)^{b_2}KLSCP$ if the peak runoff rate is q_2
where suffix 2 indicates a value of the coefficient (a) and exponent (b) at the 2 unit simulation time step. It is to note that the total runoff volume (Q) at the end of the 2 unit simulation period, is equal to the sum of the runoff volumes at the end of the 1 and 2 unit times; the peak runoff rate will be expected before 1 unit time or between 1 and 2 unit times
In either case, sediment yield is the same. Therefore,
$a_1(Q_1q_1)^{b_1}KLSCP + a_1(Q_2q_2)^{b_1}KLSCP = a_2((Q_1 + Q_2)q_1)^{b_2}KLSCP$ if the peak runoff rate is q_1
$a_1(Q_1q_1)^{b_1} + a_1(Q_2q_2)^{b_1} = a_2((Q_1 + Q_2)q_1)^{b_2}$
If there is no variation of the coefficient and exponent with small variation in simulation time step, then
$a_1 = a_2 = a$ and $b_1 = b_2 = b$

$$(Q_1q_1)^b + (Q_2q_2)^b = ((Q_1 + Q_2)q_1)^b \quad (3)$$

In the same way,
$a_1(Q_1q_1)^{b_1}KLSCP + a_1(Q_2q_2)^{b_1}KLSCP = a_2((Q_1 + Q_2)q_2)^{b_2}KLSCP$ if the peak runoff

Preprints (www.preprints.org) | NOT PEER-REVIEWED | Posted: 24 March 2022 doi:10.20944/preprints202202.0163.v2

rate is q_2
$a_1(Q_1q_1)^{b_1} + a_1(Q_2q_2)^{b_1} = a_2((Q_1 + Q_2)q_2)^{b_2}$
If there is no variation of the coefficient with small variation in simulation time step, then
$a_1 = a_2 = a$ & $b_1 = b_2 = b$

$$(Q_1q_1)^b + (Q_2q_2)^b = ((Q_1 + Q_2)q_2)^b \quad (4)$$

The equations 3 and 4 are false for a given value of the exponent **b**. In this case, the coefficient and the exponent of the MUSLE change as a change in simulation time step for a given total simulation period. The equations 3 and 4 hold true when $b = 1$ and $q_1 = q_2$, and for other values of the exponent b and $q_1 = q_2$, it is false. This implies that only one peak runoff rate is possible per storm event (i.e from the beginning of runoff to the end of the runoff from a slope field). This means sediment is transported from the beginning to the end of the runoff; the objective of the MUSLE is to estimate the total sediment load transported from the beginning to the end of the runoff. Therefore, the best theoretical exponent of the MUSLE is 1. It is a theoretical exponent because the left and right sides of the equations 3 and 4 represent the theoretical linked expressions without knowledge of observed sediment. The actual exponent of the MUSLE is estimated by applying the model at selected watersheds. From all graphs (see figures 20,21,22,23,24,25 and 26), the best actual exponent of the MUSLE is 1, which results in Nash-Sutcliffe efficiency of approximately 1 irrespective of the topographic factor and three watershed sizes (Hombole, Mojo and Gumera watersheds). Therefore, the best exponent of the MUSLE is 1. □

3. Results

It is confirmed that the best exponent of the MUSLE is 1 irrespective of the topographic factor, which results in the maximum performance of the MUSLE (i.e approximately 100%). From all graphs(see figures 20,21,22,23,24,25 and 26), if we consider one watershed, we take the exponent and topographic factor which result in the maximum Nash-Sutcliffe efficiency, but if we consider two or more watersheds, we take the exponent and topographic factor which result in the minimum Nash-Sutcliffe efficiency. Accordingly, the best exponent of the MUSLE is 0.57, which results in Nash-Sutcliffe efficiency of approximately 0.8 if the topographic factor is calculated by using the equations 1 and 2. Therefore, this is the best combination of the exponent and topographic factor of the MUSLE under hydro-climatic conditions of all watersheds under our consideration.

To find the best combination of the exponent and topographic factor, the important relationships between the coefficient and exponent **b**, the exponent **b** and Nash-Sutcliffe efficiency are drawn for the future evaluation of the MUSLE at any watershed. As we can see from the graphs (see figures 20,21,22,23,24,25 and 26), for observed and simulated sediment, as the relationship between the coefficient **a** and exponent **b** approaches to power or logarithmic function; the relationship between the exponent **b** and Nash-Sutcliffe efficiency approaches to a quadratic function. This relationship can be used to find the best performance of the MUSLE during the calibration of the model.

4. Discussion

Based on our evaluation of the soil erodibility equations, we found that the best equation to estimate soil erodibility factor is the Williams(1995) equation as cited in[106]. We considered land use maps to assign a value for the cover and conservation practice factors from the past experiences from literature, and the coefficient **a** is estimated through calibration. Since only a product effect of the coefficient, soil erodibility, cover and conservation practice factors are reflected in the MUSLE rather than their individual effect during the calibration of sediment yield, any change in these factors affects the coefficient of the MUSLE. We do not like to suggest strict procedures to estimate these factors. It is highly preferable if these factors are measured and studied at a temporal

Preprints (www.preprints.org) | NOT PEER-REVIEWED | Posted: 24 March 2022 doi:10.20944/preprints202202.0163.v2

and spatial scale to understand their effect on soil erosion in a particular field. This is because the soil erodibility, cover and conservation practice factors of the MUSLE reflect site-specific conditions. For example, we can talk about density and pattern of land cover, nature and extent of soil conservation and flood protection work, and the temporal variation of soil properties.

For all watersheds under our consideration, the best exponent of the MUSLE is 0.57, which results in Nash-Sutcliffe efficiency of 0.8 if the topographic factor is calculated by using the equations 1 and 2. In this case, the proposed exponent of the model is different from its original exponent (0.56). The best exponent of the model is 0.56, which results in Nash-Sutcliffe efficiency of 0.78 if the topographic factor is calculated by using the equation that was proposed by McCool et al. (1987) as cited in [3]. In this case, the proposed exponent is the same as the original exponent of the MUSLE (0.56), but the performance of the MUSLE decreases as compared to the previous one. Therefore, the performance of the MUSLE is very good for the previous case.

The performance of the MUSLE was tested at a watershed scale using directly measured flow data; it showed good performance (i.e the performance of the MUSLE is greater than or equal to 80%) for all four watersheds under our consideration provided that the exponent and topographic factor of the original MUSLE were changed. This result supports the literature review report that the model shows better performance at a watershed scale than a plot scale, and if it is applied using directly measured runoff data [5]. It also supports the conclusions of some authors as the MUSLE has been observed to give good results in various applications in some parts of tropical Africa (Ndomba, 2007) as cited in [8]; the MUSLE has been successfully demonstrated in sub-Saharan Africa [8]. In addition, it also supports the experimental plot result of sheet erosion at Enerta study site in Ethiopia, where the MUSLE was better at estimating soil loss from a cultivated field than the USLE [121].

5. Conclusions

In physical speaking, the MUSLE is more appropriate than USLE/RUSLE for soil erosion and sediment yield modeling. It is verified that the best exponent of the MUSLE is 1, which results in the maximum performance of the MUSLE. The performance of the MUSLE is greater than or equal to 80% for all four watersheds under our consideration, we expect the same for other watersheds of Ethiopia provided that the exponent of the model is 0.57, and its topographic factor is calculated by using the equations 1 and 2. This can be taken as the best combination of the exponent and topographic factor under hydro-climatic conditions of Ethiopia. We recommend further investigation of the best combination of the exponent and topographic factor by applying MUSLE at different watersheds of Ethiopia.

In the MUSLE, the topographic factor is directly proportional to soil erosion and sediment yield. However, as slope length becomes larger and larger, there is a possibility that erosion from the upper part of the slope gets deposited at the lower part of the slope. Therefore, more research works are required to understand the effect of slope length on soil erosion and sediment transport. The MUSLE does not account for gully erosion, streambank erosion, streambed erosion, mudflows, massive land movement due to landslides or slumps, sedimentation at floodplain, and other complex processes of soil erosion and sediment transport. Therefore, a complete assessment of the watersheds and better explanations and approaches are highly recommended.

Author Contributions: This research article is part of PhD research by Manaye Getu Tsige; Andreas Malcherek, major supervisor; Yilma Seleshi, co-supervisor

Funding: This PhD research was funded by German Academic Exchange Service: EECBP Home Grown PhD Scholarship Programme, and Universität der Bundeswehr: Scholarship and Support Program for Foreign Students and Doctoral Candidates (STIBET III) Matching Funds Scholarship

Preprints (www.preprints.org) | NOT PEER-REVIEWED | Posted: 24 March 2022 doi:10.20944/preprints202202.0163.v2

Data Availability Statement: Land use data sources are River Basin Authority of Ethiopia, Global land service, Google Earth Pro, Planet explorer, and Landsat images. Soil data sources are River Basin Authority of Ethiopia, Harmonized word soil data, field observation report from International Soil Reference and Information Centre. Climatic data from National Meteorology Agency of Ethiopia, flow and sediment data from River Basin Authority of Ethiopia, digital elevation models and Landsat image from US Geological Survey, other satellite image sources from Google Earth Pro and Planet explorer

.

Acknowledgments: We acknowledge financial support by Universität der Bundeswehr München. We also acknowledge Ms. Johanna Schmidt for language editing and LaTeX technical support.

Conflicts of Interest: The authors declare no conflict of interest.

Appendix A

Appendix A.1

Rainfall gauging stations in Upper Awash River Basin are Abebe Keranso (lat.8.978056°N and log.38.169167°E), Addis Ababa (lat. 9.01891°N and log.38.7475°E), Enselale (lat.8.937 and log. 38.44°E), Ginchi (lat.9.01667°N and log. 38.1333°E), Guranda Meta (lat.8.912°N and 38.593°E), Hombole (lat. 8.368167°N and log. 38.78°E), Kimoye (lat.9.013°N and 38.341°E),Koka Dam (lat.8.471°N and log. 39.157°E), Mojo (lat. 8.609°N and log. 39.114°E), Sebeta (lat. 8.915°N and log. 38.629°E), Sendafa (lat.9.152167°N and log. 39.0215°E), Tefki (lat. 8.846°N and log. 38.494°E), Teji (lat. 8.836°N and log. 38.375°E), Tulu Bolo (lat. 8.658°N and log. 38.211°E), Zequala (lat. 8.86667°N and log. 38.866667°E), Addis Alem (lat. 9.042°N and log.38.38333°E), Alem Tena (lat.8.29°N and log. 38.90783°E), Arbuchulele (lat. 8.47°N and log. 38.25133°E), Asgori (lat. 8.79°N, log. 38.3342°E), Bantuliben (lat. 8.6185°N and log.38.357°E), Boneya (lat. 8.7845°N and log. 38.64167°E), chefedonsa (lat. 8.97°N and log. 39.1232°E), Debrezeit (lat. 8.733333°N and log. 38.95°E), Dilela (lat. 8.63583°N and log. 38.04083°E), Dire Gidib (lat. 9.15783°N and log. 38.943°E), Ejersa Lele (lat. 8.2432°N and log.38.686°E), Welenkomi (lat. 9.001833°N and 38.254667°E).

Maximum and minimum temperature gauging stations in Upper Awash River basin Kimoye, Koka Dam, Mojo, Sebeta, Tefki, Tulu Bolo, Adis Alem, Alem Tena, Asgori, Boneya, Chefedonsa, Debrezeit and Dire Gidib.

Rainfall gauging stations in Gumera watershed are Amed Ber (lat. 11.9135°N and log. 37.8858°E), Debre Tabor station (lat. 11.8666°N and log. 37.9954°E), Gassay (lat. 11.7971°N log. 38.134497°E), Lewaye (lat. 11.72°N and log. 38.07194°E), Licha 11.651°N and 37.885°E, Mekaneyesus (lat. 11.6076 and log. 38.05422), Wanzaye (lat. 11.7862°N and log. 37.67503°E).

Maximum and minimum temperature gauging stations in Gumera watershed are Amed Ber (lat. 11.9135°N and log. 37.8858°E), Debre Tabor station (lat. 11.8666°N and log. 37.9954°E) , Gassay (lat. 11.7971°N log. 38.134497°E), Mekaneyesus (lat. 11.6076 and log. 38.05422), Wanzaye (lat. 11.7862°N and log. 37.67503°E).

Rainfall gauging stations in Gilgel Gibe 1 watersheds are Ako (lat. 8.032117°N and long. 37.20255°E), Assendabo (lat. 7.7605°N and log. 37.231117°E), Chekorsa (lat. 7.616667°N and log. 36.733333°E), Dedo (lat. 7.504233°N and log. 36.879717°E), Busa (lat. 8.7725°N and log. 38.1382°E), Dimtu (lat. 7.85°N and log. 37.2333°E), Jiren Abajifar (lat. 7.700117°N and log. 36.706367°E, Serbo (lat. 7.7°N and log. 36.966667°E), Yebu (lat. 7.68333°N and log. 36.816667°E).

Maximum and minimum temperature gauging stations in Gilgel Gibe 1 watershed are Ako (lat 8.032117°N and log. 37.20255°E), Assendabo (lat. 7.7605°N and log. 37.231117°E), Dedo (lat. 7.504233°N and log. 36.879717°E), Busa (lat. 8.78°N and log.38.14°E), Yebu (lat. 7.68333°N and log. 36.816667°E)

Preprints (www.preprints.org) | NOT PEER-REVIEWED | Posted: 24 March 2022 doi:10.20944/preprints202202.0163.v2

References

1. Kumar P.S.; Praveen T.V.; Prasad M.A., Simulation of Sediment Yield Over Un-gauged Stations Using MUSLE and Fuzzy Model. *Aquatic Procedia* **2015** , *4*, 1291–1298, doi:10.1016/J.AQPRO.2015.02.168
2. Kinnell P.I.A., A Review of the Science and Logic Associated with Approach Used in the Universal Soil Loss Equation Family of Models. *Soil systems* **2019** , , doi:10.3390/soilsystems3040062
3. Pongsai S.; Vogt D.S.; Shrestha R.P.; Clemente R.S.; Apisit E., Calibration and validation of the Modified Universal Soil Loss Equation for estimating sediment yield on sloping plots: A case study in Khun Satan catchment of Northern Thailand. *Canadian Journal of Soil Science* **2010** , *90*, 585–596, doi:10.4141/CJSS09076
4. Desmet P.J.J; Govers G., A GIS procedure for automatically calculating the USLE LS factor on topographically complex landscape units. *Journal of Soil and Water Conservation* **1996** , *51*
5. Sadeghi S.H.R; Gholami L.; Darvishan A.K.; Saeidi P., A review of the application of the MUSLE model worldwide) A review of the application of the MUSLE model worldwide A review of the application of the MUSLE model worldwide A review of the application of the MUSLE model worldwide. *Hydrological Sciences Journal* **2014** , *59*,365–375, doi:10.1080/02626667.2013.866239
6. Pandey A.; Chowdary V.M.; Mal B.C; Sediment yield modelling of an agricultural watershed using MUSLE, remote sensing and GIS. *Paddy Water Environment* **2009**, *7* , 105–113, doi:10.1007/s10333-009-0149-y
7. Benavidez R.; Jackson B.; Maxwell D.; Norton K., A review of the (Revised) Universal Soil Loss Equation ((R)USLE): With a view to increasing its global applicability and improving soil loss estimates. *Hydrology and Earth System Sciences* **2018**, *22*,6059–6086, doi:10.5194/HESS-22-6059-2018
8. Adegede A.P.; Mbajiorgu C.C., Event-based sediment yield modelling using MUSLE in north-central Nigeria. *Agricultural Engineering International: CIGR Journal* **2019**, *21*,7–17, https://cigrjournal.org/index.php/Ejounral/article/view/5231
9. Sadeghi S.H.R; Mizuyama T., Applicability of the Modified Universal Soil Loss Equation for prediction of sediment yield in Khanmirza watershed, Iran.,*Hydrological Sciences Journal* **2007**, *52*, 1068–1075, doi:10.1623/hysj.52.5.1068
10. Gwapedza D.; Slaughter A.; Hughes D.; Mantel S., Regionalising MUSLE factors for application to a data-scarce catchment. Water Resources Assessment ans Seasonal Prediction, Proceedings of the International Association of Hydrological Sciences, 2018, Copernicus GmbH, *377*, 19–24 , doi:10.5194/PIAHS-377-19-2018
11. Williams'J.R,SEDIMENT ROUTING FOR AGRICULTURAL WATERSHEDS'. *WATER RESOURCES BULLETIN* **1975** , *11*, 965–974.
12. Wischmeier W.H.; Smith D., Predicting rainfall erosion losses : a guide to conservation planning. USDA, **1978**
13. Zhang H.; Wei J.; Yang Q.; Baartman J.E.M.; Gai L.; Yang X.; Li S.; Yu J.; Ritsema C.J.; Geissen V. , An improved method for calculating slope length and the LS parameters of the Revised Universal Soil Loss Equation for large watersheds. *Geoderma* **2017**, *308* , 36–45, doi:10.1016/J.GEODERMA.2017.08.006
14. Arekhi S.; Shabani A.; Rostamizad G., Application of the modified universal soil loss equation (MUSLE) in prediction of sediment yield (Case study: Kengir Watershed, Iran. *Arab J Geosci.* **2012**, *5*, 1259–1267, doi:10.1007/s12517-010-0271-6
15. Ganasri B.P.; H. Ramesh H., Assessment of soil erosion by RUSLE model using remote sensing and GIS - A case study of Nethravathi Basin. *Geoscience Frontiers* **2016** , *7* , 953–961, doi:10.1016/J.GSF.2015.10.007
16. Kinnell P.I.A. , Event soil loss, runoff and the Universal Soil Loss Equation family of models: A review. *Journal of Hydrology* **2010** , *385* , 384–397, doi:10.1016/J.JHYDROL.2010.01.024
17. Fagbohun B.J; Anifowose A.Y.B; Odeyemi C.; Aladejana O.O.; Aladeboyeje A.I., GIS-based estimation of soil erosion rates and identification of critical areas in Anambra sub-basin, Nigeria. *Modeling Earth Systems and Environment* **2016**, *2* , doi:10.1007/s40808-016-0218-3
18. Mitasova H.; Hofierka J.; Zlocha M.; Iverson L.R., Modelling topographic potential for erosion and deposition using GIS . *International Journal of Geographical Information Systems* **1996** , *10* , 629–641, doi:10.1080/02693799608902101
19. Renard K.G.; Yoder D.C; Lightle D.T; Dabney S.M., Handbook of Erosion Modelling: Universal Soil Loss Equation and Revised Universal Soil Loss Equation. *Blackwell Publishing Ltd* **2011**.
20. Renard K.G.; Foster G.R.; Weesies G.A.; McCool D.K.; Yoder D.C. *Predicting Soil Erosion by water: A Guide to conservation Planning with the Revised Universal Soil Loss Equation*, USDA: USA, Agriculture Handbook, No 703, 404pp., 1997.
21. Baoyuan L.; Keli Z.; Yun X. , An Empirical Soil Loss Equation. Proceedings of 12th International Soil Conservation Organization Conference, Tsinghua University Press, Beijing, China, 2002, 21–25, https://www.tucson.ars.ag.gov/isco/isco12/VolumeII/AnEmpiricalSoilLossEquation.pdf
22. Tadesse A.; Dai W., Prediction of sedimentation in reservoirs by combining catchment based model and stream based model with limited data. *International Journal of Sediment Research* **2019**, doi:10.1016/j.ijsrc.2018.08.001
23. Haregeweyn N.; Melesse B.; Tsunekawa A.; Tsubo M.; Meshesha D.; Balana B.B.,Reservoir sedimentation and its mitigating strategies: a case study of Angereb reservoir (NW Ethiopia). *Journal of Soils and Sediments* **2012**, *12* , 291—305, doi:10.1007/s11368-011-0447-z
24. Devi R.; Tesfahune E.; Legesse W.; Deboch B.; Beyene A., Assessment of siltation and nutrient enrichment of Gilgel Gibe dam, Southwest Ethiopia. *Bioresource Technology* **2008** , *99* , 975–979, doi:10.1016/j.biortech.2007.03.013
25. Tully T.; Sullivan C.; Weil R.; Sanchez P., The State of Soil Degradation in Sub-Saharan Africa: Baselines, Trajectories, and Solutions. *Sustainability* **2015**, *7* , 6523–6552, doi:10.3390/su7066523
26. Hurni K.; Zeleke G.; Kassie M.; Tegegne B.; Kassawmar T.; Teferi E.; Moges A.; Tadesse D.; Ahmed M.; Degu Y.; Kebebew Z.; Hodel E.; Amdihun A.; Mekuriaw A.; Debele B.; Deichert G.; Hurni H., Soil Degradation and Sustainable Land Management

Preprints (www.preprints.org) | NOT PEER-REVIEWED | Posted: 24 March 2022 doi:10.20944/preprints202202.0163.v2

in the Rainfed Agricultural Areas of Ethiopia: An Assessment of the Economic Implications. Economics of Land Degradation (ELD) Ethiopia Case Study Report for the Economics of Land Degradation Initiative. 94 pp, 2015, accessed on 3 December 2021 from:www.eld-initiative.org
27. Tilahun S.A.; Ayana E.K; Guzman C.D.; Dagnew D.C.; Zegeye A.D.; Tebebu T.T.; Yitaferu B.; Tammo S. Steenhuis T.S. , Revisiting Storm Runoff Processes in the Upper Blue Nile Basin:The Debre Mawi Watershed. *CATENA* **2016** , 47–56, doi:10.1016/j.catena.2016.03.029
28. Moges M.M.; Abay D.; Engidayehu H., Investigating reservoir sedimentation and its implications to watershed sediment yield: The case of two small dams in data-scarce upper Blue Nile Basin, Ethiopia . *Lakes & Reservoirs: Science, Policy & Management for Sustainable Use* **2018** , *23* , 217–229, doi:10.1111/LRE.12234
29. World Bank Group, The Cost of Land Degradation in Ethiopia: A Review of Past Studies. World Bank, Washington, D.C, 2007, http://documents.worldbank.org/curated/en/2007/04/14059854/cost-land-degradation-ethiopia-review-past-studies
30. Tamene L.; Park S.J.; Dikau R.; Vlek P.L.G , Analysis of factors determining sediment yield variability in the highlands of northern Ethiopia . *Geomorphology* **2006** , *76* , 76 — 91, doi:10.1016/j.geomorph.2005.10.007
31. Haregeweyn N.; Poesen J.; Nyssen J.; Wit J.D.; Haile M.; Govers G.; Deckers S., Reservoirs in Tigray (Northern Ethiopia): characteristics and sediment deposition problems. *land degradation & development* **2006** , *17* , 211—230, doi:10.1002/ldr.698
32. Amare S.; Langendoen E.; Keesstra S.; Ploeg M. van der; Gelagay H.; Lemma H.; Zee S. E. A. T. M. van der, Susceptibility to Gully Erosion: Applying Random Forest (RF) and Frequency Ratio (FR) Approaches to a Small Catchment in Ethiopia. *Water* **2021** , *13* , doi:10.3390/w13020216
33. Haregeweyn N.; Tsunekawa A.; Poesen J.; Tsubo M.; Meshesha D.T.; Fenta A.A.; Nyssen J.; Adgo E., Comprehensive assessment of soil erosion risk for better land use planning in river basins: Case study of the Upper Blue Nile River. *Science of The Total Environment* **2017**, *574* , 95–108, doi:10.1016/j.scitotenv.2016.09.019
34. Tessema Y. M.; Jasi nska J.; Yadeta L. T.; Switoniak M.; Puchałka R.; Gebregeorgis E. G., Soil Loss Estimation for Conservation Planning in the Welmel Watershed of the Genale Dawa Basin, Ethiopia . *Agronomy* **2020**, *10* , doi:10.3390/agronomy10060777
35. Wagari M.; Tamiru H., RUSLE Model Based Annual Soil Loss Quantification for Soil Erosion Protection:A Case of Fincha Catchment, Ethiopia. *Air, Soil and Water Research* **2021**, doi:10.1177/117862212110462
36. Bekele B.; Gemi Y., Soil erosion risk and sediment yield assessment with universal soil loss equation and GIS: in Dijo watershed, Rift valley Basin of Ethiopia . *Modeling Earth Systems and Environment* **2021** , *7* , 273—291, doi:10.1007/s40808-020-01017-z
37. Gashaw T.; Tulu T.; Argaw M., Erosion risk assessment for prioritization of conservation measures in Geleda watershed, Blue Nile basin, Ethiopia. *Environmental Systems Research* **2017** , , doi:10.1186/s40068-016-0078-x
38. Frankl A.; Deckers J.; Moulaert L.; Damme A.V.; Haile M.; Poesen J.;Nyssen J., Integrated Solutions for Combating Gully Erosion in Areas Prone to Soil Piping: Innovations from the Drylands of Northern Ethiopia . *land degradation & development* **2014** , , doi:10.1002/ldr.2301
39. Balabathina V.N.; Raju R.P.; Mulualem W.; Tadele G., Estimation of soil loss using remote sensing and GIS-based universal soil loss equation in northern catchment of Lake Tana Sub-basin, Upper Blue Nile Basin, Northwest Ethiopia . *Environmental Systems Research* **2020** , *9*, doi:10.1186/s40068-020-00203-3
40. Tadesse L.; K.V. Suryabhagavan K.V.; Sridhar G.; Legesse G., Land use and land cover changes and Soil erosion in Yezat Watershed, North Western Ethiopia. *International Soil and Water Conservation Research* **2017** , *5* , 85–94, doi:10.1016/j.iswcr.2017.05.004
41. Haile G.W.; Fetene M., Assessment of Soil Erosion Hazard in kilie Catchment, East Shoa, Ethiopia. *land degradation & development* **2012** , *23* , 293—306, doi:10.1002/ldr.1082
42. Kidane M.; Bezie A.; Kesete N.; Tolessa T. ,The impact of land use and land cover (LULC) dynamics on soil erosion and sediment yield in Ethiopia . *Heliyon* **2019**, *5* , e02981, doi:10.1016/j.heliyon.2019.e02981
43. Degife A.; Worku H.; Gizaw S., Environmental implications of soil erosion and sediment yield in Lake Hawassa watershed, south-central Ethiopia. *Environmental Systems Research* **2021** , *10* , doi:10.1186/s40068-021-00232-6
44. Wolka K.; Tadesse H.; Garedew E.; Yimer F., Soil erosion risk assessment in the Chaleleka wetland watershed, Central Rift Valley of Ethiopia. *Environmental Systems Research* **2015**, *4* , doi:10.1186/s40068-015-0030-5
45. Haregeweyn N.; Tsunekawa A.; Nyssen j.; Poesen J.; Tsubo M.; Meshesha D.T.; Sch´utt B.; Adgo E.; Tegegne F., Soil erosion and conservation in Ethiopia: A review. *Progress in Physical Geography* **2015** , ,750—774, doi:10.1177/0309133315598725
46. Yesuph A.Y.; Amare Bantider Dagnew A.B., Soil erosion mapping and severity analysis based on RUSLE model and local perception in the Beshillo Catchment of the Blue Nile Basin, Ethiopia. *Environmental Systems Research* **2019** , *8*, doi:10.1186/s40068-019-0145-1
47. Aga A. O.; Chane B.; Melesse A. M., Soil Erosion Modelling and Risk Assessment in Data Scarce Rift Valley Lake Regions, Ethiopia. *Water* **2018** , *10* , doi:10.3390/w10111684
48. Gelagay H.S.; Minale A.S. ,Soil loss estimation using GIS and Remote sensing techniques: A case of Koga watershed, Northwestern Ethiopia. *International Soil and Water Conservation Research* **2016** , *4*,126-136, doi:10.1016/j.iswcr.2016.01.002
49. Lemma H.; Frankl A.; Dessie M.; Poesen J.; Adgo E.; Nyssen J., Consolidated sediment budget of Lake Tana, Ethiopia (2012–2016). *Geomorphology* **2020** , *371* , doi:10.1016/j.geomorph.2020.107434
50. Krop ačeK J.; Schillaci C.; Salvini R.; M´arKer M., Assessment of Gully Erosion in the Upper Awash, Central Ethiopian Highlands Based on a Comparison of Archived Aerial Photographs and Very High Resolution Satellite Images. *Geogr. Fis. Dinam. Quat.* **2016**, doi:10.4461/GFDQ2016.39.15

Preprints (www.preprints.org) | NOT PEER-REVIEWED | Posted: 24 March 2022 doi:10.20944/preprints202202.0163.v2

51. AN, L. S.; Liao K. H.; Zhou B. H.; Pan W.; Chen Q., Global Sensitivity Analysis of the Parameters of the Modified Universal Soil Loss Equation . *Applied Ecology and Environmental Research* **2016** , *14* , 505–514 , doi:10.15666/aeer/1404$_$505514
52. Odongo V.O; Onyando J.O.; Mutua B.M.; van Oel P.R.; Becht R., Sensitivity analysis and calibration of the Modified Universal Soil Loss Equation (MUSLE) for the upper Malewa Catchment, Kenya. *International Journal of Sediment Research* **2013** , *28* ,368–383, doi:10.1016/S1001-6279(13)60047-5
53. Fenta A.A.; Tsunekawa A.; Haregeweyn N.; Tsubo M.; Yasuda H.; Kawai T.; Ebabu K.; Berihun M.L.; Belay A.S.; Dagnenet S., Agroecology-based soil erosion assessment for better conservation planning in Ethiopian river basins. *Environmental Research* **2021** , *195* , doi:10.1016/j.envres.2021.110786
54. Kuttah D.; Sato K., Review on the effect of gypsum content on soil behavior. *Transportation Geotechnics* **2015**, *4*,28–37 doi:10.1016/j.trgeo.2015.06.003
55. Blanco-Canqui H.; Benjamin J.G.,Impacts of Soil Organic Carbon on Soil Physical Behavior. *Advances in Agricultural Systems Modeling* **2013**, *3* , doi:10.2134/advagricsystmodel3.c2
56. EKWUE E.I. , Organic-Matter Effects on Soil Strength Properties. *Soil & Tillage Research* **1990** , , 289–297.
57. Jeloudar F.T.; Sepanlou M.G.; Emadi S.M., Impact of land use change on soil erodibility. *Global J. Environ. Sci. Manage* **2018**, *4*, 59–70 , doi:10.22034/gjesm.2018.04.01.006
58. Rimmeri D.L; Greenland D.J., Effects of Calcium Carbonate on the Swelling Behaviour of a Soil Clay. *Journal of Soil Science* **1976**.
59. Matsumoto S.; Ogata S.; Shimada H.; Sasaoka T.; Hamanaka A.; Kusuma G. J., Effects of pH-Induced Changes in Soil Physical Characteristics on the Development of Soil Water Erosion. *Geosciences* **2018**, *8*, 2076–3263 ,doi:10.3390/geosciences8040134
60. Wei L.; Zhang B.; Wang M., Effects of antecedent soil moisture on runoff and soil erosion in alley cropping systems .*Agricultural Water Management* **2007**, *94*,54–62, doi:10.1016/j.agwat.2007.08.007
61. Jien S.-H.; Wang C.-S.,Effects of biochar on soil properties and erosion potential in a highly weathered soil. *CATENA* **2013**, *110*,225–233, doi:10.1016/j.catena.2013.06.021
62. Cai P.; Sun X.; Wu Y.; Gao C.; Mortimer M.; Holden P.A.; Redmile-Gordon M; Huang Q., Soil biofilms: microbial interactions, challenges, and advanced techniques for ex-situ characterization. **2019** , *Soil Ecol. Lett* ,85—93 , doi:10.1007/s42832-019-0017-7
63. Neave M.; Rayburg S., Salinity and erosion: a preliminary investigation of soil erosion on a salinized hillslope. Sediment Dynamics and the Hydromorphology of Fluvial Systems Proceedings of a symposium held in Dundee, UK, July 2006, IAHS Publ.306, 2006.
64. Razavian, S.M. and Wenby, R.B. and Fisher, T.C. and Meiselman, H.J.,Determination of Particle Sedimentation Rate by Ultrasonic Interferometry: Role of Particle Size, Density and Volume Fraction. *Biorheology* **1997**, *34* ,349–362 , doi:10.3233/BIR-1997-344-507
65. Rousseva S.; Torri D.; Pagliai M., Effect of rain on the macroporosity at the soil surface. *European Journal of Soil Science* **2002** , *53* ,83–94 , doi:10.1046/j.1365-2389.2002.00426.x
66. Dlapa P.; Hrin lk D.; Hrabovsk y A.; Šimkovic I.; Žarnovi čan H.; Sekucia F.; Koll ar J., The Impact of Land-Use on the Hierarchical Pore Size Distribution and Water Retention Properties in Loamy Soils. *12* **2020**, *Water*, doi:10.3390/w12020339
67. Lee C.-H.; Low Y.M.; Chiew Y.-M. , Multi-dimensional rheology-based twophase model for sediment transport and applications to sheet flow and pipeline scour. *Phys. Fluids 28, 053305* **2016** , doi:10.1063/1.4948987
68. Jepsen R.; Roberts J.; Lick W., Effects of Bulk Density on Sediment Erosion Rates. *Water, Air and Soil Pollution* **1997** , 21–31.
69. Jing H.; Chen G.; Wang W.; Li G., Effects of concentration-dependent settling velocity on nonequilibrium transport of suspended sediment. *Environmental Earth Sciences* **2018** , *77*, doi:10.1007/s12665-018-7731-9
70. Torri D.; Poesen J.; Borselli L.; Bryan R.;Rossi M.,Spatial variation of bed roughness in eroding rills and gullies. *CATENA* **2012** , *90* ,76–86 ,doi:10.1016/j.catena.2011.10.004
71. Sanford L.P., Modeling a dynamically varying mixed sediment bed with erosion, deposition, bioturbation, consolidation, and armoring. *Computers & Geosciences* **2008** , *34* , 1263–1283, doi:10.1016/j.cageo.2008.02.011
72. Gabet E.J.; Reichman O.J.; Seabloom E.W., The Effects of Bioturbation on Soil Processes and Sediment Transport. *Annu. Rev. Earth Planet. Sci* **2003** , *31* , 249—273 ,doi:10.1146/annurev.earth.31.100901.141314
73. Fang K.; Kou D.; Wang G.;Chen L.; Ding J.; Li F.; Yang G.; Qin S.; Liu L.; Zhang Q.; Yang Y.Decreased Soil Cation Exchange Capacity Across Northern China's Grasslands Over the Last Three Decades, *Journal of Geophysical Research: Biogeosciences* **2017** , *122* , 3088—3097, doi:10.1002/2017JG003968
74. KABA£A C.; £ABAZ B., Relationships between soil pH and base saturation – conclusions for Polish and international soil classifications . *SOIL SCIENCE ANNUAL* **2018** , *69* , 206—214, doi:10.2478/ssa-2018-0021
75. Belay A.; Claassens A.S.; Wehner F.C., Effect of direct nitrogen and potassium and residual phosphorus fertilizers on soil chemical properties, microbial components and maize yield under long-term crop rotation. *Biol Fertil Soils* **2002** , *35* , 420—427, doi:10.1007/s00374-002-0489-x
76. Boekel P.;Peerlkamp P.L., Soil consistency as a factor determining the soil structure of clay soils.*Wageningen journal of life sciences* **1956**, *4*, doi:10.18174/njas.v4i1.17792
77. Julie A. Hope and David M. Paterson and Simon F. Thrush, The role of microphytobenthos in soft-sediment ecological networks and their contribution to the delivery of multiple ecosystem services.*Journal of Ecology* **2020** , *108* , 815—830 , doi:10.1111/1365-2745.13322
78. Vaidya G.S.; MC Rillig M.C.;Wallander H., The role of glomalin in soil erosion. *Scientific World* **2011** , *9* , 82–85, doi:10.3126/sw.v9i9.5524

Preprints (www.preprints.org) | NOT PEER-REVIEWED | Posted: 24 March 2022 doi:10.20944/preprints202202.0163.v2

79. Cyco n} M.; Mrozik A.; Piotrowska-Seget, Z., Antibiotics in the Soil Environment—Degradation and Their Impact on Microbial Activity and Diversity. *Frontiers in Microbiology* **2019**, *10*, doi:10.3389/fmicb.2019.00338
80. Powlson D.S.; Hirsch P.R.; Brookes P.C. , The role of soil microorganisms in soil organic matter conservation in the tropics. *Nutrient Cycling in Agroecosystems* **2001**, *61*, 41–51.
81. Sofo A.; Mininni A. N.; Ricciuti P., Soil Macrofauna: A key Factor for Increasing Soil Fertility and Promoting Sustainable Soil Use in Fruit Orchard Agrosystems. *Agronomy* **2020** , *10* , doi:10.3390/agronomy10040456
82. Jain R.K.; Kothyari U.C., Cohesion influences on erosion and bed load transport. *Water Resources Research* **2009** , *45* , doi:10.1029/2008WR007044
83. Brunori F.; Penzo M.C.; Torri D., Soil shear strength: Its measurement and soil detachability.*CATENA* **1989** , *16* , 59–71, doi:10.1016/0341-8162(89)90004-0
84. Tadese M.; Kumar L.; Koech R.; Kogo B.K., Mapping of land-use/land-cover changes and its dynamics in Awash River Basin using remote sensing and GIS.*Remote Sensing Applications: Society and Environment* **2020** , *19* , doi:10.1016/j.rsase.2020.100352
85. Shawul A.A.; Chakma S., Spatiotemporal detection of land use/land cover change in the large basin using integrated approaches of remote sensing and GIS in the Upper Awash basin, Ethiopia. *Environmental Earth Sciences* **2019** , *78* , doi:10.1007/s12665-019-8154-y
86. Alemayehu A. Shawul and Sumedha Chakma and Assefa M. Melesse , The response of water balance components to land cover change based on hydrologic modeling and partial least squares regression (PLSR) analysis in the Upper Awash Basin. *Journal of Hydrology: Regional Studies* **2019** , *26* , doi:10.1016/j.ejrh.2019.100640
87. Bogale A. , Review, impact of land use/cover change on soil erosion in the Lake Tana Basin, Upper Blue Nile, Ethiopia . *Applied Water Science* **2020** , *10* , doi:10.1007/s13201-020-01325-w
88. Asselman N.E.M , Fitting and interpretation of sediment rating curves.*Journal of Hydrology* **2000** , *234*, 228–248, doi:10.1016/S0022-1694(00)00253-5
89. Heng S.; Suetsugi T., Comparison of regionalization approaches in parameterizing sediment rating curve in ungauged catchments for subsequent instantaneous sediment yield prediction. *Journal of Hydrology* **2014** , *512* , 240–253, doi:10.1016/j.jhydrol.2014.03.003
90. Jansson M.B. , Estimating a sediment rating curve of the Reventazón river at Palomo using logged mean loads within discharge classes. *Journal of Hydrology* **1996** , *183* , 227–241 , doi:10.1016/0022-1694(95)02988-5
91. Hapsari D.; Onishi T.; Imaizumi F.; Noda K.; Senge M., The Use of Sediment Rating Curve under its Limitations to Estimate the Suspended Load. *Reviews in Agricultural Science* **2019** , *7*, 88–101, doi:10.7831/ras.7.0_88
92. Sykes A.O., An Introduction to Regression Analysis. Coase-Sandor Institute for Law & Economics Working Paper No. 20, 1993, https://chicagounbound.uchicago.edu/law_and_economics
93. David J. Finney, A note on the history of regression. *Journal of Applied Statistics* **1996**, *23* , 555–557, doi:10.1080/02664769624099
94. Efthimiou N., The role of sediment rating curve development methodology on river load modeling.*Environmental Monitoring and Assessment* **2019**, *191* , doi:10.1007/s10661-018-7167-4
95. Doomen A.M.C.; Wijma E.; Zwolsman J.J.K.; Middelkoop H., Predicting suspended sediment concentrations in the Meuse River using a supply-based rating curve. *Hydrological Processes* **2008** , *22* , 1846–1856, doi:10.1002/hyp.6767
96. Arthur J. Horowitz, An evaluation of sediment rating curves for estimating suspended sediment concentrations for subsequent flux calculations. *Hydrological Processes* **2003** , *17* ,3387—3409, doi:10.1002/hyp.1299
97. Talebia A.; Bahrami A.; Mardian M.; Mahjoobi J., Determination of optimized sediment rating equation and its relationship with physical characteristics of watershed in semiarid regions: A case study of Pol-Doab waters . *Desert* **2015** , *20* , 135–144, doi:10.22059/JDESERT.2015.56477
98. Balamurugan G., The Use of Suspended Sediment Rating Curves In Malaysia: Some Preliminary Considerations . *Pertanika* **1989** , *12* , 367–376.
99. Chen L.; Qian X.; Shi Y., Critical Area Identification of Potential Soil Loss in a Typical Watershed of the Three Gorges Reservoir Region. *Water Resour Manage.* **2011** , *25* , 3445—3463, doi:10.1007/s11269-011-9864-4
100. David W.P., Soil and Water Conservation Planning: Policy Issues and Recommendations. *Journal of Philippine Development* **1988** , *XV* , 47–84, doi:
101. Wischmeier W.H.; Mannering J.V., Relation of Soil Properties to its Erodibility. *SOIL SCI. SOC. AMER. PROC* **1969** , *33*.
102. Morgan R.P.C.; *Soil Erosion and Conservation*, Blackwell Science Ltd, 2005, ISBN 1-4051-1781-8.
103. Schmidt S.; Tresch S.; Meusburger K., Modification of the RUSLE slope length and steepness factor (LS-factor) based on rainfall experiments at steep alpine grasslands. *MethodsX* **2019** , *6* , 219–229, doi:10.1016/j.mex.2019.01.004
104. Cole; Cooley; Dyke; Favis-Mortlock; Foster; Hanson; Jones; Jones O.R.; Kiniry; Laflen; Lyles; Nicks; Onstad; Richardson; Robertson; Sharpley; Smith; Smith F.R; Spanel; Springer; Steiner; williams, EPIC—Erosion/Productivity Impact Calculator, United States Department of Agriculture, Agricultural Research Service, Technical Bulletin Number 1768, 1990.
105. Kruk E. ,Use of Chosen Methods for Determination of the USLE Soil Erodibility Factor on the Example of Loess Slope . *Journal of Ecological Engineering* **2021** , *22* , 151—161, doi:10.12911/22998993/128861
106. Wawer R.; Nowocien E.; Podolski B., Real and Calculated K_{USLE} Erodibility Factor for Selected Polish Soils . *Polish Journal of Environmental Studies* **2005** , *14* , 655–658.
107. Wang B.; Zheng F.; Guan Y., Improved USLE-K factor prediction: A case study on water erosion areas in China. *International Soil and Water Conservation Research* **2016** , *4* , 168–176, doi:10.1016/j.iswcr.2016.08.003

Preprints (www.preprints.org) | NOT PEER-REVIEWED | Posted: 24 March 2022 doi:10.20944/preprints202202.0163.v2

108. Panagos P.; Meusburger K.; Ballabio C.; Borrelli P.; Alewell C. ,Soil erodibility in Europe: A high-resolution dataset based on LUCAS. *Science of The Total Environment* **2014** , *479-480* , 189–200, doi:10.1016/j.scitotenv.2014.02.010
109. Liu B.; Xie Y.; Li Z.; Liang Y.; Zhang W.; Fu S.; Yin S.; Wei X.; Zhang K.; Wang Z.; Liu Y.; Zhao Y.; Guo Q.,The assessment of soil loss by water erosion in China . *International Soil and Water Conservation Research* **2020** , *8* , 430–439, doi:10.1016/j.iswcr.2020.07.002
110. Moore I.D.; Wilson J.P , Length-slope factors for the Revised Universal Soil Loss Equation: Simplified method of estimation . *Journal of Soil and Water Conservation* **1992** , *47* , 423–428.
111. Wang; Liu , Effects of land use changes on soil erosion in a fast developing area.*int. J. Environ. Sci. Technol.* **2014**, *11* , 1549—1562, doi:10.1007/s13762-013-0341-x
112. Knijff van der J.M, Jones R.J.A & Montanarella L., Soil Erosion Risk Assessment in Europe. European Soil Bureau, 2000.
113. Jang C.; Shin Y.; Kum D.;Kim R.; Yang J.E.; Kim S.C.; Hwang S.I.; Lim K.J. Yoon J.-K.; Park Y.S.;Jung Y., Assessment of soil loss in South Korea based on land-cover type.*Stochastic Environmental Research and Risk Assessment* **2015**, *29* , 2127—2141, doi:10.1007/s00477-015-1027-3
114. Luo Y.; Yang S.; Liu X.; Liu C.; Zhang Y.; Zhou Q.; Zhou X.; Dong G., Suitability of revision to MUSLE for estimating sediment yield in the Loess Plateau of China.*Stochastic Environmental Research and Risk Assessment* **2016** , *30* , 379—394, doi:10.1007/s00477-015-1131-4
115. Msadala V. C.; Basson G. R., Revised regional sediment yield prediction methodology for ungauged catchments in South Africa. *Journal of the South African Institution of Civil Engineering* **2017** , *59* , 28–36 , doi:10.17159/2309-8775/2017/v59n2a4
116. Noack M.; Gerbersdorf S.U.; Hillebrand G.; Wieprecht S., Combining Field and Laboratory Measurements to Determine the Erosion Risk of Cohesive Sediments Best. *Water* **2015** , *7* , 5061-5077, doi:10.3390/w7095061
117. Li J.; Wang W.; Guo M.; Kang H.; Wang Z.; Huang J.; Sun B.; Wang K.; Zhang G.; Bai Y., Effects of soil texture and gravel content on the infiltration and soil loss of spoil heaps under simulated rainfall. *Journal of Soils and Sediments* **2020**, *20* , doi:10.1007/s11368-020-02729-6
118. Sadeghi S.H.; Mizuyama T.; Vangah B.G., Conformity of MUSLE Estimates and Erosion Plot Data for Storm-Wise Sediment Yield Estimation. *Terr. Atmos. Ocean. Sci.* **2007** , *18* , 117–128.
119. Kinnell P.I.A., Why the universal soil loss equation and the revised version of it do not predict event erosion well. *HYDROLOGICAL PROCESSES* **2005**, *19* , 851—854, 10.1002/hyp.5816
120. Ndomba, Modelling of Sedimentation Upstream of Nyumba Ya Mungu Reservoir in Pangani River Basin. *Nile Basin Water Science and Engineering Journal* **2010**, *3*, 25—38.
121. Muche H.; Temesgen M.; Yimer F., Soil loss prediction using USLE and MUSLE under conservation tillage integrated with 'fanya juus' in Choke Mountain, Ethiopia. *International Journal of Agricultural Sciences* **2013**, *3*,46–52 https://internationalscholarsjournals.org/print.php?article=soil-loss-predictionusing
122. Soil Conservation Service, *Geologic Investigation for Watershed Planning*, USDA, Technical Release No. 17 Geology, 1966, https://directives.sc.egov.usda.gov/OpenNonWebContent.aspx?content=18602.wba
123. Williams J.R; Berndt H.D., Sediment Yield Prediction Based on Watershed Hydrology, *ASAE* **1977**, 1100–1104 doi:10.13031/2013.35710
124. USDA, Agricultural Research service. Available online: http://www.ars.usda.gov/Research/docs.htm?docid=6010 (accessed on 20.01.2020)
125. Stanchi, S.; Zecca, O.; Hudek, C.; Pintaldi, E.; Viglietti, D.; D'Amico, M.E.; Colombo, N.; Goslino, D.; Letey, M.; Freppaz, M. Effect of Soil Management on Erosion in Mountain Vineyards (N-W Italy). *Sustainability* **2021**, *13*, 1991. https://doi.org/10.3390/su13041991